Title

The Antiproton-Nucleon Annihilation Process, II

Authors

Chamberlain, Owen
Goldhaber, Gerson
Jauneau, Louis
et al.

Publication Date

1958-08-01

UCRL 8424

UNIVERSITY OF CALIFORNIA

Radiation Laboratory

BERKELEY, CALIFORNIA

DISCLAIMER

UCRL-8424

UNIVERSITY OF CALIFORNIA

Radiation Laboratory
Berkeley, California

Contract No. W-7405-eng-48

THE ANTIPROTON-NUCLEON ANNIHILATION PROCESS. II.

Owen Chamberlain, Gerson Goldhaber, Louis Jauneau,
Theodore Kalogeropoulos, Emilio Segrè, and Rein Silberberg

August 18, 1958

Printed for the U.S. Atomic Energy Commission

THE ANTIPROTON-NUCLEON ANNIHILATION PROCESS. II.

Contents

Contents (cont'd)

THE ANTIPROTON-NUCLEON ANNIHILATION PROCESS. II.

Owen Chamberlain, Gerson Goldhaber, Louis Jauneau,
Theodore Kalogeropoulos, Emilio Segrè, and Rein Silberberg

Radiation Laboratory and Department of Physics
University of California, Berkeley, California

August 18, 1958

ABSTRACT

We have continued work on antiproton interactions in photographic emulsions. Most of the data come from an exposure at the Bevatron to an enriched antiproton beam of 700 Mev/c momentum. In this paper we present the analysis of 221 antiproton stars, 95 of which occurred in flight. We find an antiproton cross section of $(1.9 \pm 0.2)\ \sigma_0$, where $\sigma_0 = \pi (1.2 \times 10^{-13} A^{1/3})^2$ cm^2, for all the elements in emulsion, excluding hydrogen. The primary antiproton annihilation gives rise to 5.36 ± 0.3 pions on the average. Of these pions, 1.3 and 1.9 interact with the nucleus for the stars at rest and in flight respectively. For stars at rest the energy available in the annihilation in complex nuclei is divided up among the products as follows: charged pions, 48 ± 6%; neutral particles (other than neutrons and K^0 mesons) 28 ± 7%; K mesons 3 ± 1.5%; and cascade nucleons and nuclear excitation 21 ± 12%. For the stars in flight the corresponding percentages are: 45 ± 7%, 22 ± 7%, 3 ± 1.5% and 30 ± 2%. To fit the average pion multiplicity, the interaction radius of the Fermi statistical model must be taken as $2.5 \hbar/m_\pi c$. Other proposals to explain the large multiplicity are discussed. We deduce from the fraction of pions interacting in the same nucleus that the annihilation takes place at the outer fringes of the nucleus.

THE ANTIPROTON-NUCLEON ANNIHILATION PROCESS. II.*

Owen Chamberlain, Gerson Goldhaber,† Louis Jauneau,§
Theodore Kalogeropoulos, Emilio Segrè, and Rein Silberberg

Radiation Laboratory and Department of Physics
University of California, Berkeley, California

August 18, 1958

I. INTRODUCTION

In the "Antiproton Collaboration Experiment" (ACE)[1] the antiproton-nucleon annihilation process was discussed on the basis of an analysis of 36 antiproton stars. We have carried out further exposures of nuclear emulsions in the antiproton beam at the Bevatron, in particular with an enriched beam, which have yielded 185 additional antiproton stars.[2] In this paper we discuss the analysis of these 221 antiproton stars.[3]

By use of the separated beam the ratio of antiprotons to background of minimum-ionizing particles, which was initially $1/(5 \times 10^5)$, becomes $1/(5 \times 10^4)$; the background particles are now mainly μ mesons and electrons.

The antiprotons enter the emulsion stack with a momentum of 700 ± 20 Mev/c. At this momentum they have a grain density $g/g_o \simeq 2$ and are easily distinguishable from the background of minimum particles. They can either interact in flight or, after traversing a range of 13 ± 2 cm of emulsion, interact at rest. Details on the exposure geometry and beam separation and composition are given in Appendix I, and those on track-following and prong-measuring techniques and criteria in Appendix II. Of the 221 antiproton stars discussed here 95 occurred in flight, thus yielding information on the antiproton cross section; the 126 remaining stars occurred after the antiprotons "came to rest." We considered an interaction to occur at rest when no evidence for any residual momentum could be obtained from measurements on the antiproton track at the annihilation star. In this work the lowest measurable kinetic energy was $T_{\bar{p}} \simeq 10$ Mev. The analysis is carried out separately for the stars at rest and in flight, as well as for the two cases combined.

---

*Work done under the auspices of the U.S. Atomic Energy Commission.

†Supported in part by the Miller Institute of Basic Research, University of California, Berkeley, California.

§Now at Ecole Polytechnique, Paris, France.

The general features of the antiproton annihilation process are similar to those discussed in ACE. With the improved statistics, however, we have found a reduction of the $K\bar{K}$ abundance.

On the basis of this work we understand the annihilation process for our combined (i.e., stars at rest and stars in flight) sample in complex nuclei to proceed as follows: The antiproton annihilates with a nucleon and $\langle N_\pi \rangle = 5.36 \pm 0.3$ pions are emitted on the average with an average total energy of $\langle E_\pi \rangle = 350 \pm 18$ Mev per pion. In $3.5 \pm 1.5\%$ of the interactions a $K\bar{K}$ pair is emitted. An average number $\nu = 1.6 \pm 0.1$ of the annihilation pions interact with that nucleus in which the annihilation occurs, giving rise to nuclear excitation and nucleon emission. Some of the interacting pions are absorbed and some lose energy owing to inelastic scattering. The average number of protons emitted per annihilation is $\langle N_H \rangle = 4.1 \pm 0.3$, and the corresponding total average energy release in protons and neutrons is $U = 490 \pm 40$ Mev. Of the ν interacting pions (1-a) $\nu = 0.4$ are inelastically scattered. This degrades the primary pion energy to $\langle E_\pi \rangle = 339 \pm 18$ Mev, which is the observed average pion energy. On reasonable assumptions for the efficiency of charged-pion detection, $\epsilon = 0.90 \pm .05$, we calculate the number of neutral pions in good agreement with charge independence. There is thus very little leeway in the present data for an additional singlet π^0 with intensities comparable to the π^0 from the $\pi^+\pi^0\pi^-$ triplet unless we ascribe to this hypothetical particle an interaction very different from the normal π^0. We observe a difference in the number of pion interactions for stars at rest and in flight, which we interpret as a deeper penetration into the nucleus by antiprotons in flight.

The pion multiplicity $\langle N_\pi \rangle$ does not agree with the Fermi statistical model directly if we assume the normal interaction volume Ω_0 of radius $r_0 = \hbar/m_\pi c$. As in ACE, agreement can, however, be obtained with the Fermi statistical model in which the pion interaction radius is taken to be $2.5\ \hbar/m_\pi c$. We call this the normalized Fermi statistical model. Thus except for the $K\bar{K}$ abundance the normalized Fermi model gives good agreement with all the detailed features of the experimental data. However, the present statistical accuracy and the errors arising from the difficulties in dealing with complex nuclei do not permit us to rule out other multiplicity distributions giving the same value for $\langle N_\pi \rangle$.

Many authors have criticized--and for good reasons--this direct application of Fermi's model, and have proposed several modifications which would yield a high multiplicity even with normal values for the volume.[4-10] Among the factors to be taken into account are the nonadiabatic nature of the annihilation with respect to the period of the pionic clouds, the interaction of the escaping pions, and conservation theorems neglected in Fermi's model and others. In spite of these attempted refinements we still do not have a complete theory of the annihilation process.

II. THE ANNIHILATION CROSS SECTION

By following the antiprotons along the track we obtain the mean free path for annihilation with the nuclei in the photographic emulsion (see Appendix II for details). In the work reported here, combined with ~3 meters of track studied in ACE, a total of 17.6 m of identified antiproton track length was followed. In this track length 95 annihilation events in flight have been observed (including 20 events from ACE). We have made a special effort in this work to determine the energy of the interacting antiproton even when it was low. Both integral gap-length measurements and constant-sagitta measurements were made on all antiprotons that appeared to be coming to rest (see Appendix II). By these means we were able to detect interaction in flight down to a residual range of $\gtrsim$ 0.5 mm, which corresponds to $T_{\bar{p}} \gtrsim 10$ Mev. For kinetic energies above 40 Mev (residual range $\simeq$ 6 mm) interactions in flight can be detected reliably by inspection. Six such events were observed in the energy region $10 < T_{\bar{p}} < 40$ Mev. Table I gives the details of the path-length distribution and the number of annihilation events observed. In principle, data such as those shown in Table I should allow us to determine the annihilation mean free path as a function of antiproton kinetic energy. Unfortunately it is not possible, with the presently available statistics, to discern reliably any energy dependence of the cross section. The attractive Coulomb field will, in a classical picture,[11] deflect the incoming antiprotons so as to increase the cross section by a factor $1 + V_c/T_{\bar{p}}$. Here V_c is the Coulomb potential evaluated at a nuclear radius corresponding to the antiproton cross section at energies $T_{\bar{p}} \gg V_c$. In emulsion, for the heavy elements we have $V_c = 9$ Mev and for the light elements $V_c = 2.5$ Mev. In addition, owing to nuclear effects, a 1/v law might be expected at energies where only s waves are important, i.e., for $\lambda\!\!\!^{-} > R$, where R is the interaction radius. The corresponding energy is $T_{\bar{p}} < 1$ Mev even for the light elements C, O, and N in the emulsion. In this work we would thus not have distinguished interactions at 1 Mev from those occurring after the antiprotons are bound in atomic orbits.

The over-all mean free path in nuclear emulsions, we now find, is $\lambda\!\!\!^{-}_{\bar{p}} = 18.6 \pm 2$ cm, which corresponds to an average energy of $\langle T_{\bar{p}} \rangle \simeq 140$ Mev. In terms of an average cross section (excluding the hydrogen content in emulsions)

this can be expressed as $\sigma_{\bar{p}_2} = (1.9 \pm 0.2)\,\sigma_0$, where σ_0 is given by $\sigma_0 = \pi\,(1.2 \times 10^{-13})^2 A^{2/3}\,\mathrm{cm}^2$. Actually we do not expect the $A^{2/3}$ law to hold strictly for antiproton interactions. The errors quoted are the statistical standard deviations only, and do not include the small systematic errors due to contamination by positive protons (see Appendix II).

A description of the elastic and inelastic scattering processes from complex nuclei as well as the elastic scattering from hydrogen, for the present antiproton sample, has been published.[12, 13]

Table I

The distribution of antiproton path length, number of annihilation events, and mean free path in emulsion with antiproton energy[a]

$T_{\bar{p}}$ (Mev)	Path length (cm)	Number of annihilation events	Mean free path (cm)
10-40	81	6	13.5^{+9}_{-5}
40-70	147	3	49.0^{+56}_{-24}
70-100	207	11	18.8^{+9}_{-5}
100-150	512	35	14.6^{+4}_{-2}
150-200	728	34	21.6^{+4}_{-3}
200-230	90	6	15.0^{+10}_{-5}
10-230	1764	95	18.6 ± 2.0

[a]In this compilation we have not included path length on P events (as this would introduce a small contamination of positive protons) although the three interactions with $N_{\pi}^{\pm} = 0$ and $\Sigma E_H < T_{\bar{p}}$ are included (see Appendix II). Corrections for these effects (which have not been applied) would decrease the cross section by $2 \pm 1\%$.

III. THE PRODUCTS FROM THE ANNIHILATION STARS

A. Pions

1. The Charged-Pion Multiplicity

The observed charged-pion multiplicity distribution is given in Fig. 1. The average values are: $\langle N_{\pi^\pm} \rangle = 2.50 \pm 0.26$ at rest; $\langle N_{\pi^\pm} \rangle = 2.30 \pm 0.28$ in flight; and $\langle N_{\pi^\pm} \rangle = 2.41 \pm 0.19$ all combined.[14] In these figures no corrections have been made for the presence of possible additional $\bar{P}_\rho$ events, estimated at 2^{+3}_{-2} % of the stars at rest. Neither have we corrected for the possible presence of positive protons and antiproton charge-exchange events, which we estimate as 2 ± 1% in the sample of the stars in flight (see Appendix II for details on these estimates).

2. The Pion Spectrum

To obtain the pion spectrum we have carried out multiple-scattering and grain-count measurements on all prongs that do not end in the emulsion, with dip angle $\beta \leqslant 20^\circ$. This serves to identify the prongs as light mesons (considered as pions) and also to give their energy (from $p\beta$). For pions in the same dip-angle interval that come to rest, the range-energy relation was used for determining their energy. We noted, however, that some residual distortion effects were present even after application of the third-difference method in the $p\beta$ determination. The distortion effects tend to reduce the value of the average energy $\langle T_\pi \rangle$ of the pion spectrum. In order to minimize these effects in the pion spectrum, we limit ourselves to only those pions with dip angle $\lesssim 15^\circ$. The resulting spectra at rest, in flight, and all combined are given in Fig. 2. To obtain the best value of the average pion energy $\langle T_\pi \rangle$, two correction terms, w_1 and w_2, have to be added to the raw values $\langle T_\pi \rangle_{raw}$ obtained experimentally. The first correction term, w_1, is a correction for residual distortion effects even after limiting ourselves to only those with dip angle $\beta \lesssim 15^\circ$. This was estimated by comparing $\langle T_\pi \rangle_{raw}$ for various pion dip-angle intervals, and gives $w_1 = 10 \pm 5$ Mev. The second correction term, w_2, is due to the energy dependence of the charged-pion detection efficiency. As described in Appendix III, we find $w_2 = 7 \pm 2$ Mev.

The over-all correction is thus an increase of 17 Mev or roughly 10%, which we apply to each value of $\langle T_\pi \rangle_{raw}$. Table II gives the average pion energies, raw and corrected, for charged-pion multiplicity $N_{\pi^\pm} = 1\text{-}2, 3$, and

4-6, for stars at rest, in flight, and combined. We note a dependence on $N_{\pi}\pm$, indicating that the stars with low $N_{\pi}\pm$ are due, in part, to low values of N_{π}, and thus have higher average energies. The corresponding values computed from the Fermi statistical theory are also given (see Section IV C).

3. The π^+/π^- Ratio

All pions of grain density $g/g_0 \lesssim 1.3$ ($T_{\pi} \lesssim 90$ Mev) were followed systematically in this experiment (see Appendix II). Of those pions followed, 76 came to rest, giving either the π-μ-e decay characteristic of positive pions (22 cases) or the σ star and ρ endings characteristic of negative pions (53 cases). In one case the sign of the pion charge could not be determined. The study of these ending prongs provides the best direct evidence for our identification of the emitted particles as π mesons (see Appendix IV for details).

In the energy interval 20 Mev $\leqslant T_{\pi} \leqslant$ 100 Mev we obtained a π^+/π^- ratio of $(\pi^+/\pi^-)_{\text{experiment}} = 20/44 = 0.45 \pm 0.12$. The corresponding energy spectra of the pions whose charges were identified are given in Fig. 3. To interpret our observed π^+/π^- ratio, we must remember that we have this information only for the low-energy part of the entire pion spectrum, and that the probability of pion escape from the emulsion stack increases with increasing energy. Thus, since we cannot determine the sign of the charge of a pion leaving the stack, even within the energy interval considered here, the fraction of pions whose sign can be identified decreases rapidly with increasing energy. In the energy region where identification of sign is possible we observe a mixture of pions from the primary annihilation process and pions that have undergone inelastic scattering in the parent nucleus. Considering the annihilation of an antiproton with a bound nucleon, we observe that in a $\bar{p}$ + "p" annihilation we have $\pi^+/\pi^- = 1$, while in a $\bar{p}$ + "n" annihilation π^+/π^- is 0.56. These values follow directly from charge conservation. In annihilation with a neutron, the number of negative pions must exceed by one the number of positive pions. If we take the average primary number of charged pions as 2/3 $\langle N_{\pi} \rangle \simeq 3.5$ we obtain the above result, i.e. $\pi^+/\pi^- = 1.25/2.25 = 0.56$. Thus in the emulsion nuclei, taking into account the $\langle n/p \rangle$ ratio, we expect $\pi^+/\pi^- = 0.76$ for those pions due to the

Table II

The average experimental pion kinetic energy as a function of the observed charged-pion multiplicity. Also shown for comparison are the values computed from the normalized Fermi statistical model.

	At rest				In flight				Combined			
$N_\pi \pm$	No. of pions $\leq 15^o$ dip	$\langle T_\pi \rangle_{raw}$ (Mev)	$\langle T_\pi \rangle$ (Mev)	$\langle T_\pi \rangle_{Fermi}^{(a)}$ (Mev)	No. of pions $\leq 15^o$ dip	$\langle T_\pi \rangle_{raw}$ (Mev)	$\langle T_\pi \rangle$ (Mev)	$\langle T_\pi \rangle_{Fermi}^{(a)}$ (Mev)	No. of pions $\leq 15^o$ dip	$\langle T_\pi \rangle_{raw}$ (Mev)	$\langle T_\pi \rangle$ (Mev)	$\langle T_\pi \rangle_{Fermi}^{(a)}$ (Mev)
1-2	31	194	211	220	13	294	301	230	44	220	237±33	224
3	36	163	180	199	32	195	212	204	68	178	195±27	201
4-6	26	158	175	170	12	155	172	179	38	152	169±36	172
1-6	99[b]	167	184±21	195	65[b]	204	221±30	206	164[b]	172	199±18	200

[a] Details on the Fermi-model values are given in Section IV C.

[b] These numbers include some pions from events occurring near an emulsion interface for which no $N_\pi \pm$ value was assigned (see Appendix III).

annihilation process directly. Below 20 Mev this ratio will be reduced by the Coulomb effect. For the pions scattered inelastically we can note from experimental data (see Appendix VI for details):

(a) that negative pions are scattered from emulsion nuclei with higher probability than positive pions;

(b) that the negative pion spectrum peaks at a lower energy than the positive one. The inelastically scattered pions in this energy interval thus tend to have a low π^+/π^- ratio, which we estimate as $\simeq 0.22$. In addition we estimate, taking into account the energy dependence of the probability of pion escape from the emulsion stack, that $\simeq 27\%$ of the pions in the energy interval discussed here are due to inelastic pion scattering. The over-all expected ratio is thus estimated as $(\pi^+/\pi^-)_{calc} = 0.58$. This is within one standard deviation of the observed ratio in the same energy interval.

4. Angular Distributions

a. Pion-emission angles

If we examine the angular distribution of the pions relative to the antiproton direction we obtain an isotropic distribution for the stars at rest as expected (Fig. 4a). For the stars in flight (Fig. 4b) we do not observe any anisotropy other that what is expected owing to the center-of-mass motion. The forward-backward ratio in flight is $F/B = 1.22 \pm 0.17$, compared with $F/B = 1.33$ expected from the center-of-mass motion of the antiproton-nucleon system.

b. Pion-pion angle distribution

From the dip- and projected-angle measurements performed on all charged mesons we have computed the angle $\phi_{\pi\pi}$ between each charged pion pair. We must remember here that the neutral pions are not observed in this work, that $\simeq 0.8$ charged pion is absorbed per star on the average, and that some are scattered inside the nucleus before emission.

In Fig. 5 we give the distribution of all the charged pion-pion angles $\phi_{\pi\pi}$, plotted against $\cos \phi_{\pi\pi}$. We have examined this distribution for stars at rest and in flight separately and also as a function of $N_{\pi^\pm}$. We have not observed any pronounced difference for these various cases and are thus presenting the combined distribution. Table III gives the ratio γ of the number of pion-pion angles larger than 90° to those smaller than 90°.

As can be seen from Fig. 5 and Table III, pair angles $> 90^{\circ}$ are preferred. This may be attributed simply to conservation of momentum and energy, as can be seen by the following oversimplified geometrical argument. Assume all momenta equal in magnitude. Then for each value of N_{π} we can compute the average pion-pair angle $\langle \phi_{\pi\pi} \rangle$ for the symmetrical situation which automatically conserves momentum. Thus for $N_{\pi} = 2$ we obviously get $\langle \phi_{\pi\pi} \rangle = 180^{\circ}$, and $N_{\pi} = 3, 4$, and 6 we get the angles for the equilateral triangle tetrahedron and cube--i.e., $\langle \phi_{\pi\pi} \rangle = 120^{\circ}$, 109.5°, and 108° respectively. Thus we see that energy-momentum conservation leads to values for $\langle \phi_{\pi\pi} \rangle > 90^{\circ}$ or ratios $\gamma > 1$.

Pion-pion forces could influence this distribution, but no complete calculation of this problem has been done.

B. K Mesons

The percentage of stars emitting K mesons is smaller than earlier estimates of $\sim$10% indicated[1,2] (the estimate now is $3.5 \pm 1.5\%$). From work with stacks No. 72 and No. 78 we feel that the identity of K mesons could not be uniquely established for dip angles $> 30^{\circ}$. We have thus estimated lower and upper limits to the number of stars with K mesons. Table IV gives some of the relevant data on the K mesons together with the reliability of the identification (see also Appendix V). For the lower limit we take the actual number of stars with definitely identified K mesons of dip $\lesssim 30^{\circ}$, namely three. Since this corresponds to only half the total available solid angle, the expected number of stars is six. In the upper limit we have included all stars with prongs that might possibly be K mesons, namely nine. To deduce the total number of stars with $K\bar{K}$ pairs, allowance must now be made for $K\bar{K}$ production in which no charged K meson is emitted from the nucleus. Here we get a contribution from $K^0\bar{K}^0$ pairs, which is estimated at $\sim$16% of all the stars with $K\bar{K}$ pairs,[15] and from $K^0\bar{K}^-$ pairs in which the K^- meson is absorbed by the nucleus, estimated at $\sim$8% of all stars with $K\bar{K}$ pairs. We thus obtain the estimate that $3.5 \pm 1.5\%$ of all antiproton stars emit $K\bar{K}$ meson pairs. Evidence for a pair of charged K mesons was obtained in one case only (event No. 3-3).[1] If we consider the possibility of antiproton annihilation in the presence of a second nucleon, we may also expect the reaction

$$\bar{p} + N + N \longrightarrow Y + K + n\pi ,$$

Table III

Ratio γ_o of the number of pion-pion angles greater then 90^o to those smaller than 90^o, and the average pion-pion angle $\langle\phi_{\pi\pi}\rangle$, as a function of charged pion multiplicity.

$N_{\pi^\pm}$	At rest			In flight			Combined		
	No. of pairs	γ	$\langle\phi_{\pi\pi}\rangle$	No. of pairs	γ	$\langle\phi_{\pi\pi}\rangle$	No. of pairs	γ	$\langle\phi_{\pi\pi}\rangle$
2	35	1.19	90	16	1.89	100	61	1.44	94.2
3	103	1.13	94	84	1.90	98	186	1.41	95.8
4	114	1.59	97	48	1.53	99	162	1.57	98.1
5	50	1.50	101	30	1.50	97	80	1.50	99.6
6	15	1.14	86	15	0.88	94	30	1.00	89.8
2-6	316	1.34 ±.15	95.5 ±5.4	203	1.64 ±.24	97.7 ±6.9	519	1.45 ±.13	96.6 ±4.3

Table IV

Data on K mesons (including ambiguous cases) from antiproton stars

Event no.	Prong no.	Dip angle (degrees)	Available path (cm)	T_K (Mev)	Terminal behavior	Comments
3-3	8	15	2.47	80	disappears in flight	definite K[a]
3-25	1	30	5.3	104	decays at rest	definite K see Appendix V
3S-59	2	29	8.3	235	leaves stack	definite K
3S-83	5	23	4	355	leaves stack	uncertain identification
3-7	3	19	3.5	260	leaves stack	uncertain identification[a]
2-3	2	44	1.9	175	leaves stack	uncertain steep[a]
3S-3	3	74	7.8	120	comes to rest; nothing at end	uncertain steep
3S-71	3	67	1.5	102	star in flight	uncertain steep
3S-86	3	64	1.7	195	star in flight	uncertain steep
3-3	11	74	4.0	195	leaves stack	uncertain steep[a]

[a] From Ref. 1

which would give rise to fast-hyperon production. In ACE, evidence for one possible fast Σ was presented, and we have found one other possible case of a Σ^+ ($T_\Sigma \simeq 250$ Mev).

From the above estimate of the abundance of $K\bar{K}$ meson pairs we can evaluate the average energy per star in $K\bar{K}$ mesons. If we take $\langle E_K \rangle = 650$ Mev, this gives $\langle \Sigma E_{K\bar{K}} \rangle = 50 \pm 25$ Mev. It should be noted that this small amount of $K\bar{K}$ pair production is inconsistent with the Fermi statistical theory, which--even for the large volume needed to give agreement with the pion multiplicity--gives $\sim 12\%$ of $K\bar{K}$ meson production. However, some of the modifications of Fermi's theory mentioned earlier give this lower ratio if special modifications for the K meson interactions are introduced. Moreover the K interactions with pions and nucleons could materially alter the statistical equilibrium postulated in Fermi's model. In Section IV C we have taken the Fermi statistical theory with $r = 2.5 \hbar/m_\pi c$ (without considering K-meson production).

C. Nucleons

1. The Charged Prongs

We have made energy measurements on all the protons emitted from the 221 antiproton stars analyzed here. For prongs of range ≤ 1 cm no attempt was made to distinguish protons from deuterons or alpha particles, and energies have been assigned on the assumption that the prongs are protons. We observe a clear-cut correlation between the number of charged pions emitted, $N_{\pi^{\pm}}$, and the number of heavy prongs emitted, N_H, in the sense that a lower number of pion prongs corresponds to a higher number of nuclear prongs. The latter are to be interpreted as being due to the interaction of pions.

For purposes of further analysis, we have classified the prongs as evaporation protons for $T_p < 30$ Mev and as knock-on protons for $T_p \geq 30$ Mev. Thus we have $N_H = N_{EV} + N_{KO}$.

In Table V we give the averages for the number of heavy prongs emitted per star $\langle N_H \rangle$, the energy per prong $\langle E_H \rangle$, and energy per star $\langle \Sigma E_H \rangle$, as a function of the charged-pion multiplicity. The entries in Table V show very clearly that the energy per heavy prong can be considered constant, $\langle E_H \rangle = 43.4$ Mev for all cases, and that the only correlation occurring is between the charged-pion multiplicity and the number of heavy prongs emitted. This suggests that the mechanism for nucleon emission is due to pion interactions.

Figure 6 gives the distribution of the energy per star in heavy prongs, ΣE_H.

Figure 7 gives the heavy-prong distribution.

Figure 8 gives the energy spectrum of the heavy prongs, for all stars combined. We observe a break in the spectrum at about 7 Mev; this is due to the influence of the Coulomb barrier on the emission of charged particles. This break would be more pronounced if alpha particles and deuterons included in the first two points were subtracted.

The experimental spectrum can be fitted empirically by the expression

$$dN_H/dT_H = KT_H^{-a},$$

where N_H is number of heavy prongs per star, and T_H is the kinetic

Table V

The average values for the number of heavy prongs, the energy per heavy prong, and the energy in heavy prongs per star.

Interaction	$N_\pi \pm$	No. of stars	No. of heavy prongs			Energies (in Mev)[a]					
						Per prong			Per star		
			$\langle N_{EV} \rangle$	$\langle N_{KO} \rangle$	$\langle N_H \rangle$	$\langle E_{EV} \rangle$[b]	$\langle E_{KO} \rangle$	$\langle E_H \rangle$	$\langle \Sigma E_{EV} \rangle$[b]	$\langle \Sigma E_{KO} \rangle$	$\langle \Sigma E_H \rangle$
At rest	0-2[d]	56	2.8	1.3	4.1	17.1	109.5	45.5	48.4	136.8	185.2
	3	32	2.1	0.9	3.0	16.8	98.8	43.0	34.7	95.7	130.4
	4-6	25	1.4	0.4	1.8	15.1	121.2	39.2	20.4	48.5	68.9
	0-6	126[c]	2.30	1.03	3.33	17.0	103.0	43.4	39.1	105.4	144.5
In flight	0-2[d]	45	4.8	2.1	6.9	17.3	108.2	43.5	83.2	216.8	300.0
	3	30	3.3	1.2	4.5	16.3	105.1	39.6	54.4	126.1	180.5
	4-6	11	1.2	0.7	1.9	15.8	82.5	41.2	18.7	60.0	78.7
	0-6	95[c]	3.55	1.54	5.09	18.0	101.8	43.3	63.9	156.4	220.3
All combined	0-2[d]	101	3.7	1.6	5.3	17.2	108.9	44.6	63.9	172.4	236.3
	3	62	2.7	1.1	3.8	16.6	101.8	41.4	44.2	110.4	154.6
	4-6	36	1.3	0.5	1.8	15.3	109.4	39.8	19.9	52.0	71.9
	0-6	221[c]	2.83	1.24	4.07	17.4	102.5	43.4	49.5	126.9	176.4

[a] These energies include a binding energy of 8 Mev per prong.

[b] The energies were assigned on the assumption that all prongs were protons. Actually deuterons and alpha particles are also present, and a correction for this effect is made later.

[c] These numbers include the events occurring near the surface of the emulsion ($\Delta Z < 20$ μ), for which no pion multiplicity was assigned. (See Appendix III.)

[d] No $\bar{p}_\rho$ events have been included. These amount to 2^{+3}_{-2} % of all stars at rest. (See Appendix II.)

energy in Mev. Here we have $K = 2$ and $\alpha = 1.26$ for $10 < T_H < 100$ Mev; and $K = 222$ and $\alpha = 2.28$ for $T_H > 100$ Mev. The experimental data for stars at rest and in flight separately show the same energy dependence, and the intensities are in the ratio of the corresponding $\langle N_H \rangle$ values.

Also shown in Fig. 8 are three points which were computed by using the results of Metropolis et al.[16] for the cascade protons due to π^+ and π^- interaction with Ru^{100}. Although a number of assumptions and approximations are made besides the assumptions in the calculations by Metropolis et al., the agreement is quite satisfactory. It should be noted that similar discrepancies between experiment and the Monte Carlo calculations have been observed for π^- absorption in emulsion.[16]

2. Energy Given to Neutrons

The problem now is to find, from the energy used for emission of heavy prong (considering them as protons), what the corresponding energy is for emission of all nucleons. For the evaporation prongs, this is fairly well established. We can use the average number of evaporation prongs $\langle N_{EV} \rangle$ and the relation that the total energy release per charged evaporation prong is 50 Mev.[17] This estimate is in excellent agreement with a direct calculation[18] similar to the one carried out in ACE. For the knock-on prongs the energy used in neutron emission is not so easily established. In ACE it was assumed that the energy used for emission of knock-on neutrons is simply determined by the $\langle n/p \rangle$ ratio in emulsion, viz $\langle n/p \rangle = 1.2$, giving the value $U_{KO} = 2.2 \langle \Sigma E_{KO} \rangle$. However, if we consider the recent calculations by Metropolis et al.[16] on nuclear cascades initiated by pions, it appears that neutrons are preferentially emitted to the extent of $n/p \simeq 1.6$ when averaged over our pion energy spectrum and when a π^+/π^- ratio of 0.76 is assumed (see Section IIIA). This would give $U_{KO} = 2.6 \langle \Sigma E_{KO} \rangle$. The total energy given off in nucleons can be expressed as $U_H = h \langle \Sigma E_H \rangle$, where h is the factor we are trying to determine. On the two assumptions above we would get $h = 2.4$ or 2.7 respectively.

Aside from the approach utilizing $\langle \Sigma E_H \rangle$, we can also consider another one, utilizing $\langle N_H \rangle$. As the energy release by nucleon emission comes from pion interactions in the residual parent nucleus, what we are really interested in is this number of interacting pions ν.

In Appendix VI we have compiled the available evidence on prong number from pion interactions in emulsions. Averaging over our pion spectrum we get $n_H = 2.5 \pm 0.2$ as the number of heavy prongs produced per pion interaction. As shown in Section III C this evidence is also in good agreement with $h = 2.7$. In what follows we have adapted the value $h = 2.7 \pm 0.2$.

3. Correlation Between ΣE_H and $N_{\pi^\pm}$

In Fig. 9a we give a correlation plot between ΣE_H and $N_{\pi^\pm}$. This further illustrates the correlation between pion absorption and energy emission in heavy prongs. In Fig. 9b we give the average values $\langle N_{\pi^\pm} \rangle$ for various intervals of ΣE_H. As can be seen, $\langle N_{\pi^\pm} \rangle$ decreases systematically from a maximum value at $0 \leqslant \Sigma E_H < 40$ Mev. This maximum value can be used to compute $\langle N_\pi \rangle$ by neglecting absorption (see Eq. (6'), Section IV A).

D. Electrons

1. Dalitz Pairs

From the total number of charged mesons observed, and assuming charge independence, we expect that a total of $\sim 290\ \pi^0$ mesons have been emitted by the 221 antiproton stars considered here. We thus expect 290/80 = 3.6 Dalitz pairs. We have observed one case. The electron energies are 20 ± 5 Mev and 120 ± 25 Mev, respectively, and the space angle between them is 49°.

2. Atomic Electrons and β Decay of the Residual Nucleus

We have observed a number of low-energy electrons associated with the annihilation stars. It should be noted, however, that because of the high electron component in the incident beam (Stack 78) the probability for chance correlation is not negligible. In Table VI we give the energy distribution of the observed electrons.

Electrons are to be expected in annihilation stars from the following effects:

(a) Atomic electrons from Auger effect in the cascading of the antiproton to lower orbits, conversion electrons from nuclear gamma rays.

(b) Nuclear electrons due to formation of radioactive fragments.

Table VI

The energy distribution of electrons from antiproton annihilation stars.[a]

Electron energy	Number of electrons	
	Star at rest	Star in flight
15-30 kev	6	3
30-100 kev	8	2
100-500 kev	4	2
500-1000 kev	1	0
1-5 Mev	0	2
5-10 Mev	0	2

[a] This table does not include the two electrons of the Dalitz pair.

IV. ANALYSIS AND DISCUSSION

A. Evaluation of "Best Fit" Values

In the preceding sections we have presented the experimental data on the 221 antiproton stars. The main purpose of this section is to give a consistent picture of the antiproton annihilation by separating the primary event, such as can be seen in a hydrogen annihilation, from the secondary phenomena due to the pion interactions with the nucleus. We use the experimental data to evaluate the "best fit" average values for the derived quantities $\langle E'_\pi \rangle$, $\langle N_\pi \rangle$, ν, U, and $\epsilon^{-1}(\pi^{\pm o}/\pi^{\pm})$, whose definitions are given in Table VII. We carry out this evaluation by giving six equations, which relate the above five derived quantities to other quantities measured in this experiment and also to data compiled from pion experiments (see Appendix VI). These equations are based on a simple balance of energy and number of particles. For convenience we define all terms and give their numerical values, errors, and sources in Table VII. The six equations are:

$$\nu = \langle N_H \rangle / n_H \tag{1}$$

$$U = h \langle \Sigma E_H \rangle \tag{2}$$

$$U = \nu \left\{ \langle E'_\pi \rangle + w_0 - (1-a) E_0 \right\} \tag{3}$$

$$\langle N_\pi \rangle = (\langle W \rangle - \langle \Sigma E_{K\bar{K}} \rangle) / \langle E'_\pi \rangle \tag{4}$$

$$\langle E_\pi \rangle = \left\{ (\langle E'_\pi \rangle - w)(\langle N_\pi \rangle - \nu) + (1-a)\nu E_0 \right\} / (\langle N_\pi \rangle - a\nu) \tag{5}$$

$$\langle N_\pi \rangle = \epsilon^{-1} (\pi^{\pm o}/\pi^{\pm}) \langle N_{\pi^\pm} \rangle + a\nu \tag{6}$$

In these equations we have assumed that the average π^o energy is equal to the average $\pi^\pm$ energy. We have not, however, assumed a specific value for the ratio $\pi^{\pm o}/\pi^\pm$.

Equation (1) is based on an experimental determination of the heavy-prong number from pion interactions in nuclear emulsions (see Appendix VI).

Equation (2) is obtained empirically and is based on evaporation and cascade calculations as discussed in Section III C. Equations (3), (4), and (6) have already been discussed in ACE. Equation (3) has been modified to take into account the fact that the average energy of the interacting pions is higher by w_0 Mev than the average primary pion energy. The correction term w_0 comes in because the pion mean free path in nuclear matter is energy-dependent, and thus absorption and scattering take place preferentially at the higher energies. An estimate for w_0 is based on the pion interactions calculated for the observed pion spectrum. Equation (5) states how the average pion energy emitted from stars in complex nuclei is related to the primary energy. The term $E'_\pi - w$ represents the average energy of the primary spectrum after ν pions have interacted. It should be noted that the equation giving the overall energy balance as expressed in terms of the experimental quantities is implicit in the above six equations.

We now take Eqs. (1)-(5) for the four derived quantities $\langle E'_\pi \rangle$, $\langle N_\pi \rangle$, ν, and U. This represents an overdetermined system of equations. We solve this system by successive approximations to obtain the "best fit" values for these four derived quantities in terms of the four experimental quantities $\langle N_H \rangle$, $\langle \Sigma E_H \rangle$, $\langle W \rangle$, and $\langle \Sigma E_{K\bar{K}} \rangle$, and the five quantities coming from the evaluation of pion-interaction experiments, n_H, h, a, E_0, and w_0. These best-fit values for the stars at rest, in flight, and both combined are given in Table VII. Using these best-fit values for $\langle N_\pi \rangle$ and ν, we can now solve for $\epsilon^{-1}(\pi^{\pm 0}/\pi^\pm)$ from Eq. (6).

It should be noted that unless we make explicit assumptions on the values of $(\pi^{\pm 0}/\pi^\pm)$ this does not allow us to solve for ϵ directly. On the other hand, however, we can use the estimated value for the efficiency $\epsilon = 0.9 \pm 0.05$, which then gives us $\pi^{\pm 0}/\pi^\pm = 1.56 \pm 0.16$ for all stars combined. This value for $\pi^{\pm 0}/\pi^\pm$ is in good agreement with the value 3/2 expected from charge independence. If charge independence is accepted, the above result sets a limit on the presence of any other neutral particle in the annihilation process.

In addition, we can give a relation which holds for the stars with low energy release in heavy prongs, $\Sigma E_H \leq 40$ Mev. For these stars (43 at rest and 17 in flight), to a good approximation, no pion absorption took place. We thus obtain the lower limit

$$\langle N_\pi \rangle \geq \epsilon^{-1} (\pi^{\pm o}/\pi^{\pm}) \langle N_{\pi^{\pm}} \rangle_0 \qquad (6')$$

Using Eq. (6'), we obtain the value $\langle N_\pi \rangle \geq 5.2 \pm 0.7$ for all stars combined, on the assumption of charge independence, i.e., $\pi^{\pm o}/\pi^{\pm} = 3/2$, and with the estimated value for ϵ. This determination of $\langle N_\pi \rangle$ does not involve the details of the processes occurring in the complex nuclei.

All the above considerations have neglected pion production by interacting pions. Making an overestimate of this effect, where we assume that 5% of the ν interacting pions give rise to secondary pion production,[19] we obtain a 1.5% reduction in $\langle N_\pi \rangle$. We thus feel justified in neglecting this effect.

It can be noted from Table VII that the average pion multiplicity is essentially the same for the stars at rest and in flight, although the secondary interactions of the pions differ appreciably. The number of interacting pions and the corresponding energy given to cascade nucleons and nuclear excitation is larger by a factor of $\sim$1.5 for the interactions in flight. Table VIII gives the energy balance for the antiproton annihilation in complex nuclei. The energy given to the various types of particles is expressed in percentage of the total available energy, $\langle W \rangle$.

Table VII

Definition of the quantities used in Eqs. (1)-(7) together with their numerical values, errors, and sources.

Symbol	Definition	At rest	In flight	Combined	Source
A. Input Data from This Experiment					
$\langle W \rangle$	Average total energy available per star in annihilation (Mev)	1868	2009	1927	Dirac theory and measurement of $\bar{p}$ kinetic energy
$\langle E_\pi \rangle$	Average total pion energy (Mev)	324±21	361±30	339±18	Direct measurements with estimated (~5%) corrections
$\langle \Sigma E_H \rangle$	Average energy per star used for heavy-prong (proton) emission (Mev)	144.5±15	220.3±26	176.4±13	Direct measurements, considering heavy prongs as protons
$\langle \Sigma E_{K\bar{K}} \rangle$	Average total energy used per star for $K\bar{K}$ pair production (Mev)	50±25	50±25	50±25	Direct measurements and estimates
$\langle N_H \rangle$	Average number of heavy prongs per star	3.33±.34	5.09±.60	4.07±.31	Direct measurements
$\langle N_{\pi^\pm} \rangle$	Observed average charged-pion multiplicity	2.50±.26	2.30±.28	2.41±.19	Direct measurements
$\langle N_{\pi^\pm} \rangle_0$	Observed average pion multiplicity for stars with $\Sigma E_H \lesssim 40$ Mev	3.07±.45	3.35±1.0	3.15±.41	Direct measurements

Table VII (cont'd)

Symbol	Definition	Rest flight combined			Source
B. Input Data from Pion Experiments and Calculations					
a	Fraction of interacting pions absorbed	← .75±.03 →			Estimated from pion-interactions experiments averaged over observed pion spectrum
E_0	Average final total energy of inelastically scattered pions (Mev)	← 215±15 →			Estimated from pion-interactions experiments averaged over observed pion spectrum
n_H	Average number of heavy prongs per nonelastic pion interaction	← 2.5±0.2 →			Estimated from pion-interactions experiments averaged over observed pion spectrum
h	Ratio of total energy given to nucleons to the total energy given to protons	← 2.7±.2 →			Estimated from evaporation theory and experiments and from calculations on pion-initiated cascades
w	Energy correction term due to pion interactions (Mev)	5±2	8 ± 3	6±2	Auxiliary quantity based on observed pion spectrum and pion m.f.p. in nuclear matter.
w_0	Energy correction term due to pion interactions related to w by $w_0=w(\langle N_\pi \rangle - \nu)/\nu$ (Mev)	15±6	13±5	14±5	Auxiliary quantity based on observed pion spectrum and pion m.f.p. in nuclear matter.

Table VII (cont'd)

Symbol	Definition	At rest	In flight	Combined	Source
C. Derived Quantities					
$\langle E'_\pi \rangle$	Average primary total pion energy (Mev)	337±21	367±25	350±18	Best-fit evaluation of Eqs. (1)-(6)
U	Average energy per star used for proton and neutron emission (Mev)	393±36	612±45	491±37	Best-fit evaluation of Eqs. (1)-(6)
$\langle N_\pi \rangle$	Average pion multiplicity	5.39±34	5.33±40	5.36±28	Best-fit evaluation of Eqs. (1)-(6)
ν	Average number of interacting pions	1.32±.14	1.93±.14	1.61±.12	Best-fit evaluation of Eqs. (1)-(6)
$\epsilon^{-1}(\pi^{\pm o}/\pi^{\pm})'$	ϵ^{-1} is the efficiency correction factor. $(\pi^{\pm o}/\pi^{\pm})$ is the average ratio of all pions to the number of charged pions	1.76±.23	1.69±.27	1.72±.18	Best-fit evaluation of Eqs. (1)-(6)

Table VIII

The energy balance. The distribution of the energy among the various particles emitted in the antiproton annihilation in complex nuclei (for charged-pion detection efficiency $\epsilon = 0.9$). All energies are expressed as percentage of the total available energy $\langle W \rangle$.

Energy given to	At rest	In flight	Combined
Charged pions	48 ± 6	45 ± 7	46 ± 5
Neutral particles other than neutrons and K^0 mesons	28 ± 7	22 ± 7	25 ± 5
K mesons	3 ± 1.5	3 ± 1.5	3 ± 1.5
Cascade nucleons (p and n) and nuclear excitation	21 ± 2	30 ± 2	26 ± 1

B. Penetration of the Antiprotons into the Nucleus

We have made an estimate of the antiproton penetration depth D into nuclear matter. Considering further the oversimplified corpuscular model discussed in ACE, we obtain an estimate of the annihilation position for interactions in flight ($\langle T_{\bar{p}} \rangle$ = 140 Mev) as follows: the position at which the annihilation occurs is a small region in the nucleus where, on the average, $\sim$ 5 pions are released. We call that average distance from the center of the nucleus the annihilation radius R_a. If R_a were much smaller than the nuclear radius, the pions would have to traverse a sizable amount of nuclear matter and many would interact before leaving the nucleus. If R_a is large, compared to the nuclear radius, only a small number of pions would interact. In order to obtain some numerical results from this model, we have considered a nuclear density distribution given by

$$\rho = \rho_0 \left[1 + e^{\frac{r-R}{a}} \right]^{-1}$$

where $R = r_0 A^{1/3}$, and we have taken $r_0 = 1.07 \times 10^{-13}$ cm and $a = 0.5 \times 10^{-13}$ cm.[20] Using the mean free path for pions in nuclear matter given by Frank, Gammel, and Watson,[21] we have calculated the fraction of interacting pions - $\langle f \rangle$. This fraction averaged over the pion-energy spectrum and the elements in the nuclear emulsion was calculated[22] for values of R_a from 0.8 R to 1.4R and is given in Fig. 10a. We now take our "best fit" values for the fraction of interacting pions from antiproton stars in flight $\nu / \langle N_\pi \rangle = 0.36 \pm 0.04$ (marked F in Fig. 10a) and obtain $R_a/R = 1.02 \pm 0.02$. To reach the position R_a, the antiproton must penetrate the outer (low-density) regions of the nucleus. Figure 10b gives this penetration, suitably averaged, in nucleons per cm^2, for the above density distribution.

We thus obtain an average penetration $D = (9.3 \pm 1.0) \times 10^{24}$ nucleons/cm^2. Finally we can estimate the mean free path of antiproton annihilation in nuclear matter. For the $\bar{P}$ - H interaction at $T_{\bar{p}} \simeq 140$ Mev, the annihilation cross section is roughly equal to the elastic-scattering cross section,[23] while the elastic scattering is strongly forward peaked.[12, 24] The elastic scattering will thus be strongly suppressed inside nuclear matter by the Pauli principle. The mean free path of antiproton annihilation will consequently be only slightly larger than the penetration depth (we estimate it to be ~5% larger). This mfp gives us an average annihilation cross section with the bound nucleons σ, of about 102 ± 12 mb. Here the errors quoted are the statistical errors only and do not reflect the reliability of the model.

In the case of the antiproton stars at rest, the estimate of the annihilation radius R_a can be obtained as above. On the basis of $\nu / \langle N_\pi \rangle = 0.24 \pm 0.03$ we compute $R_a/R = 1.10 \pm 0.02$. However the interpretation of the penetration into the nucleus is quite different. Here the annihilation takes place from the Bohr orbits of the antiproton around the nucleus in which the antiproton is captured. R_a is thus dependent on the overlap integrals between the antiproton atomic orbits and the nuclear-density distribution.

As the antiproton nucleon annihilation cross section and the fraction of absorbed pions become better known, it may be possible to use this information to explore the outermost region of the nucleus.

C. Comparisons with the Fermi Statistical Model

As was shown in ACE, a direct computation of the antiproton-annihilation process on the basis of the Fermi statistical model[25] leads to a low pion multiplicity and a high $K\bar{K}$ abundance. However, by changing the only parameter available, the radius of the elementary reaction volume, from $r_0 = \hbar/m_\pi c$ to $r = 2.5r_0$ a good fit to the observed pion multiplicity can be obtained. Whereas there is a physical justification for the value of r_0, we cannot find a good one for the present value of r. This change of parameter is therefore to be considered only as a device to adapt the model to the experimental results. However, even with this change, when compared with our present results on the $K\bar{K}$ meson pair abundance, the value still comes out too high (about 12% is predicted, while 3.5 ± 1.5% is observed). It must be remembered here that there is the implicit hypothesis in the statistical model that K mesons come to equilibrium with the pions, which assumes a similar interaction strength.

A number of different proposals have been made in an attempt to avoid the large reaction volume required to fit the experimental data in the Fermi statistical theory and to give physical reasons for the experimental results. Koba and Takeda[4] have considered the annihilation process to be a two-step process. The first step is that the cores of the nucleon and antinucleon annihilate in a short time, $\simeq \hbar/2M_p c^2$, with the emission of $\sim$2.2 pions on the average. In the second step, the pion clouds are emitted giving rise to $\sim$ 2.6 pions. Thus this model gives $\langle N_\pi \rangle = 4.8$, if the production of $K\bar{K}$ pairs is neglected.

Another approach is to consider the possibility of pion-pion interactions in the final state, as suggested by Dyson[26] in connection with the 0.9 Bev resonance in π-p scattering. The effect of such pion-pion interaction is to raise the average pion multiplicity as obtained from the Fermi statistical model. This approach was discussed recently by Eberle[5] and independently by Goto.[6] Both authors made calculations based on the formulation of the statistical model as given by Belen'kii.[7] Eberle uses the saddle-point approximations of Fialho[27] and obtains $\langle N_\pi \rangle = 4.4$, but needs the further assumption of a smaller interaction volume (radius of $\sim\hbar/M_K c$) for $K\bar{K}$

production. Goto treated single pions as extreme relativistic and K mesons, and the pion pairs in the isobar state, as nonrelativistic. In order to obtain agreement with the experimental values of $\langle N_\pi \rangle$, he finds that he requires either (a) a large interaction volume, $\Omega = 10\Omega_0$ (the feature that he was trying to avoid by making the additional assumption of a pion-pion interaction) or (b) rather high-spin resonant states. Consequently, one can conclude that these calculations change $\langle N_\pi \rangle_{\text{theor.}}$ in the desired direction. But that in addition further stipulations, as yet not fully established, are required to give agreement with the experimental results. Furthermore, Kretzschmar,[8] Srivastava and Sudarshan,[9] and Yajima and Kobayakawa[10] have published additional modifications of the statistical model.

We will take an approach here, similar to the one taken in ACE, of empirically choosing a reaction radius so as to fit the experimental average-pion multiplicity. We thus obtain the set of probabilities for the various pion multiplicities (neglecting $K\bar{K}$ production) given in Table IX. We can now examine in more detail the experimental data in terms of this empirically normalized Fermi statistical model. As is to be expected, we obtain good agreement for

(a) the pion spectrum,

(b) the charged-pion multiplicity, and

(c) the average pion energies as a function of $\langle N_{\pi^\pm} \rangle$.

In each of these cases we can start from the predictions of the normalized Fermi statistical model (i.e., the percentage P_i of stars with $N_\pi = i$ mesons, and with the corresponding momentum distribution). To compare the statistical model with the experimental pion spectrum, we must take into account the effects of absorption, inelastic scattering, and the energy dependence of the pion-detection efficiency. Curves A and B in Fig. 11 give the computed spectrum before and after the above effects were considered. For the multiplicity and the average energy we must consider the transformation from the system dealing with all pions, to the system dealing with the charged pions only. Here again, the effects of absorption and efficiency must be considered. Figure 12 gives the computed and experimental values for the charged-pion multiplicity. The average pion energies are given in Table II together with the experimental values.

In conclusion then, it can be said that the multiplicity distribution as obtained from the normalized Fermi theory can be considered as a good working model for the true distribution.

Table IX

Distribution of pion multiplicity P_i' according to the Fermi statistical model normalized for an interaction radius of $r = 2.5 \hbar/m_\pi c$. Also given are computed normalized primary pion energies.

N_π	P_i'	At rest E_π^{*a} Mev	In flight E_π^{*a} Mev
2	0.0	934	1004
3	2.3	622	670
4	13.4	467	502
5	40.6	374	402
6	33.1	311	335
7	10.6	267	287
$\langle N_\pi \rangle$	5.36	—	—

[a] E_π^* is obtained from $E_\pi^* = \langle W \rangle / N_\pi$. This neglects the effect of $K\bar{K}$ production which is also neglected in the P_i' values. If $K\bar{K}$ production is included we would also have P_i' values $\neq 0$ for $N_\pi = 0, 1$, and 2. The E_π^* values would have to be modified accordingly.

D. Further Remarks

1. Comparison with $\bar{p}$-H annihilation

We can compare our results with the recent work on antiproton annihilation in the 15-inch hydrogen bubble chamber.[28] In the case of hydrogen, the situation is much simpler in that no absorption effects by the residual nucleus are present. To date, about 85 $\bar{p}$ - H annihilation events have been observed by the hydrogen bubble-chamber group. Our results are within the statistical error of the results obtained for $\bar{p}$-H annihilations, where it was found that $\langle N_\pi \rangle$ equals 4.7 ± 0.5 and $\langle E'_\pi \rangle$ equals 374 ± 25 Mev.

2. Annihilation events with no charged prongs

By examining the entrance criteria and range distribution of the antiproton tracks, we have estimated the presence of those annihilation events having no charged products, i.e., $\bar{p}_\rho$ events at 2^{+3}_{-2}% of the stars at rest (see Appendix II). Such events are to be expected for antiproton annihilations in which only neutral pions are emitted with either no pion absorption or, if pion absorption occurs (in which case the absorbed pion(s) could also be charged), no charged prongs are emitted.[29] The creation of a $K^0\bar{K}^0$ pair having possibly one or two additional neutral pions could also give rise to $\bar{p}_\rho$ events.

From isotopic-spin considerations, taking into account pion absorption, we estimate that $\sim$ 1% of the stars at rest should show no charged prongs. This estimate is consistent with the estimate of experimental abundance. In addition, T. D. Lee[30] mentioned the possible existence of an additional interesting effect that could give rise to $\bar{p}_\rho$ events. Lee postulated that if time reversal does not exist, then nucleons must be "left-handed" and "right-handed," and that our world consists predominantly of one kind. In antiproton production one would thus obtain "left-handed" and "right-handed" $\bar{p}$-p pairs. The antiprotons of the "opposite handedness" to our world would thus be noninteracting and would appear as $\bar{p}_\rho$ events. From the present data we can limit such an effect to a rather small percentage and can certainly rule out equal production of the two kinds of antiprotons.

ACKNOWLEDGMENTS

We are indebted to Mr. L. Agnew, Dr. E. J. Lofgren, Dr. H. Steiner and Dr. C. Wiegand who have given freely of their time to make the exposure of photographic emulsions possible. We are very grateful to Mr. J. Glass, Mrs. F. Glenn, Mr. D. H. Kouns, Mrs. L. Langner, Mrs. E. Rorem, Mrs. E. Russell, Mrs. M. L. Santos, Miss C. Scales, and Mrs. L. Shaw for their constant assistance and help throughout this work.

APPENDIX I. THE ENRICHED ANTIPROTON BEAM

Of the two stacks discussed in this paper, the first (Stack 72) was exposed to an unseparated antiproton beam in a geometry identical to that described previously.[1,31] Stack 72 yielded 16 antiproton stars. The second stack (Stack 78) was exposed in the enriched antiproton beam (December 1956) described below. This stack consisted of 200 Ilford G.5 emulsions (15 by 23 cm by 600 μ). It was exposed at the Bevatron for a total integrated proton flux of 4×10^{13} protons on a carbon target. The antiproton emission angle in the laboratory system was about 0°. Stack 78 yielded 169 antiproton stars.

In Fig. 13 we show the exposure geometry. The entire trajectory was inside a series of helium-filled bags in order to reduce multiple scattering. The principle of the beam separation is as follows: A beam of 819-Mev/c negative particles is selected from the target in the Bevatron by use of an 8-in. quadrupole magnet Q1 and the analyzing magnet M1 (the magnet D takes care of some finer steering effects). This beam, having a momentum spread of $\pm 4\%$, is brought to a horizontally dispersed distribution of sharp images at F 1. The 4-in. quadrupole magnet L acts as a field lens. At F 1 we have placed a wedge-shaped LiH absorber (19.8 g/cm^2, median thickness), which alters the momenta of antiprotons and pions by different amounts so that they can be separated. The resulting momenta are 700 Mev/c for protons, and 777 Mev/c for pions. The wedge shape of the LiH absorber (maximum difference in thickness is 4 g/cm^2) preserves the momentum spread in the antiproton beam at $\pm$ 4%. The quadrupole magnet Q 2 has the function of refocusing the beams of different momenta at F 2, whereas the analyzing magnet M 2 separates the focal spots by about 6 in. The magnet system is so designed that although there is a horizontal momentum spread of $\pm$ 4% at F 1, the beam is refocused to a final image at F 2 by allowing the dispersion introduced by M2 to cancel that introduced by M1. The general arrangement of magnets and quadrupoles is the same as that used in a counter experiment[32] except for the introduction of the wedge absorber and a final magnet, Mc, which was added just ahead of the second focus. Magnet Mc had the effect of deflecting positive particles, which are produced by edge scattering of the pion beam as it traverses the last quadrupole away from the stack.

The beam separation, computed for the position of the stack shown in Fig. 13 is given in Fig. 14 as a function of the LiH absorber. The amount of absorber used (19.8 g/cm^2) produces a beam separation in the above geometry of about 6 in. The antiproton attenuation is due to multiple scattering, which makes part of the beam miss the quadrupole Q 2, and to the nuclear interactions in the LiH absorber. Figure 15 gives the computed attenuation factor as a function of the beam separation. To find the antiproton reduction factor, F, we write

$$F = \left[1 - \exp\left(-\psi^2{}_0/\psi^2\right)\right] \exp\left(-x/\lambda\right),$$

where ψ_0 is the aperture angle of the quadrupole, Q 2, ψ the mean multiple-scattering angle, λ is the mean free path for antiprotons in LiH (this mean free path corresponds to the total antiproton cross section down to an angle of 1°), and x is the thickness of LiH in g/cm^2. For the total antiproton cross section, we have used the values 3 and 4 times σ_0, where

$$\sigma_0 = \pi \left(1.2 \times 10^{-13} A^{1/3}\right)^2 \text{ cm}^2.$$

The problem involved in obtaining a separated antiproton beam is to reduce to as low a level as possible the number of background light particles (i.e., particles at a minimum or plateau value on the ionization curve) which occur at the same geometrical position as that at which the antiprotons are focused.

In Fig. 16a we show a horizontal profile of the main meson beam together with a "tail" in the region where the separated antiprotons are to be focused. Figure 16b shows the corresponding distribution with the LiH absorber in position. This corresponds to the actual condition during the exposure. The position at which the stack was placed is also indicated on this figure. The correspondence of the grid coordinates, as printed on the stack, and the coordinates of this figure are such that the y coordinate of 125 mm corresponds to a beam separation of 15 cm. This is the center of the focused antiproton beam. The stack was deliberately placed 50 mm off center to avoid an excessive number of background particles at one edge.

Figure 17 gives the horizontal beam distribution as observed in Stack 78. Both the light-particle flux and the antiproton flux are given. Figure 18 gives the vertical-beam distribution.

The composition of the light particle beam (π^-, μ^-, and e), which appears as background to the antiproton beam in Stack 78, was obtained as follows: The density of π^--meson stars was obtained by area scanning in this stack. By comparing this density with the light-particle flux, we found that ~4% of this flux consisted of pions. By counting the number of light particles across one plate in the beam direction, we obtained the characteristic increase in intensity due to electron multiplication. Figure 19 shows the resulting distribution plotted in units of the radiation length in the emulsion. From the position and height of the maximum in the shower curve, we find that about half the remaining light particles must be electrons; the rest, then, are μ^- mesons. The separation was thus very effective in removing the pions, but still leaves a large number of electrons and μ^- mesons as contaminants of the antiproton beam. Figure 20 gives the range distribution of the stopping antiprotons as a function of entrance position in the stack.

The ratio of antiprotons to light particles (π^-, μ^-, and e^-) at the leading edge of the stack is $1/(5 \times 10^4)$. This number, when compared with the exposures at 700 Mev/c, shows an improvement factor in this ratio of about 10.

APPENDIX II. DETAILS ON THE EXPERIMENTAL TECHNIQUES

A. Track Following, Entrance Criteria and Positive Proton Contamination

As in ACE the antiproton tracks were picked up 5 mm from the leading edge and followed along the track until they either interacted in flight or came to rest. Interactions in flight were only accepted after a track had traversed at leat 2 cm in the stacks. This allowed some path length to eliminate possible spurious events. The path length followed was only accepted for mean-free-path determinations beyond this 2 cm cut-off. Prospective antiproton tracks were picked up on the basis of grain count and angular criteria. Figure 21 gives the correlation between entrance angles (relative to the local minimum particle direction) and the deviation from the average range $|\bar{R} - R|$ for all particles of protonic mass coming to rest. As can be seen from the figure (which was made for Stack 78) all identified antiproton tracks lie inside a rectangle with $\theta_{rel} < 3^{o}$ and $|\bar{R}-R| < 2.4$ cm. On the other hand, particles not giving any visible energy release on coming to rest (p_{ρ}) are distributed over a much larger region.

The p_{ρ} particles lying outside the rectangle marked in the figure must therefore be positive protons. If we assume a uniform distribution for the positive protons (p^{+}) we would expect to find 4 ± 0.7 p^{+} inside the rectangle. Actually we have observed 7 p_{ρ} events inside this rectangle, two of which occur at the surface of the emulsion, where minimum secondaries might have been missed.[33] We thus estimate that $\bar{p}_{\rho}$ events (antiproton-annihilation events at rest with no charged prongs) account for 2^{+3}_{-2} % of all stars at rest.[28] In addition we get an effect on the interactions in flight: With 5 to 7 positive proton tracks present inside the rectangle of Fig. 21, and with 10 tracks outside the rectangle but with $\theta_{rel} < 3^{o}$, representing in all a path length of ~115 cm, we expect about 3 p^{+} interactions in flight. These act as a contamination for the $N_{\pi} = 0$ annihilation stars in flight. In this work three stars in flight have been observed with $N_{\pi} = 0$ and $\Sigma E_{H} < T_{\bar{p}}$. These could be p^{+} stars $\bar{p}$ charge-exchange events, or actual $\bar{p}$ annihilation stars. The three events[34] are described in Table X. Also we must consider that from the known $\bar{p}$ charge-exchange cross section of ~4 mb per nucleus,[35] we would expect 0.5 event as a result of this process. In all, we can thus estimate that 2 ± 1 of the 95 stars in flight considered here are <u>not</u> due to antiproton annihilations. The two above effects thus are in opposite directions when all stars combined are considered, and the estimated values just cancel.

Table X

Details on three stars in flight whose identity as antiproton annihilation stars could not be established. There are two other possible interpretations for all or some of those stars: (1) antiproton charge-exchange reactions or (2) (positive) proton interactions.[a]

Event Number	$T_{\bar{p}}$ (Mev)	ΣE_H (Mev)	N_{EV}	N_{K0}
5-1[b]	150	91	4	1
3S-141	186	51	3	0
3S-113	187	171	9	0

[a] In all the analysis these three stars have, however, been treated as annihilation stars.

[b] From ACE Ref. (1).

The kinetic energy of an antiproton at interaction was measured by one of the following methods, depending on the energy:

(a) For antiprotons with residual range $R_{resid} > 5$ cm the average range $\bar{R}$ from Fig. 20a was used to obtain the kinetic energy.

(b) For antiprotons with $0.6 < R_{resid} < 5$ cm the energy was determined by opacity measurements.

(c) For antiprotons with $0.5\text{mm} \leq R_{resid} \leq 6\text{mm}$ a combination of constant sagitta and integral gap-length measurements was carried out. In order to establish whether or not the annihilation occurred in flight, all antiprotons appearing to come to rest ($T_{\bar{p}} \leq 40$ Mev) were measured.

B. Measurements on the Prongs

We used various measuring techniques for the prongs from the annihilation stars depending on the ionization and the dip angle. Projected- and dip-angle measurements have been made for all prongs. For $g/g_o < 1.3$, grain count, measurements were made on all tracks whereas $p\beta$ measurements using 3rd-difference methods (when needed) have been made for tracks with dip angle $\leq 20^o$. Except for one energetic electron pair, all these prongs with dip angle $\leq 20^o$ were light mesons, considered as pions (see also Appendix IV). We have considered all the steeper prongs as pions also. All the prongs were followed for a sufficient length to eliminate low-energy electrons (<10 Mev). For $g/g_o \geq 1.3$ all prongs were followed, and identification and energy measurements were made by standard emulsion techniques. The end points of all prongs ending in the emulsion stack were examined carefully for possible decay secondaries. No attempt was made to distinguish alphas, deuterons and tritons from protons for ranges $R_H \leq 1$ cm. For $R_H > 1$ cm and dip angle $\leq 40^o$, opacity measurements were made. These measurements identified one deuteron, and one particle was either a deuteron or a Σ particle.

APPENDIX III. THE CHARGED-PION DETECTION EFFICIENCY

The efficiency of pion detection depends on the ionization of the pion, the position of the star relative to the surfaces of the individual emulsions, and possibly on the pion dip angle. We have investigated the dependence of efficiency on position, and we have concluded that it is necessary to exclude from considerations involving $N_{\pi^\pm}$ all stars whose distance from either surface is less than 20μ in the processed emulsion. On this basis 22 stars (14 at rest and 8 in flight) have been eliminated from some of the analysis. They have, however, been included in all other evaluations without assigning a specific pion multiplicity to them.

Several observers have carefully examined all the antiproton stars independently and have recorded all the prongs. Out of a total of 450 pions (Stacks 72 and 78), 59 pions have been missed by one or more of the observers. All pions missed were of grain density $g/g_o < 1.2$.

The recent work on the apparent asymmetry of π-μ decay as observed in emulsions has revealed a peculiar bias inherent in dip-angle measurements as made in photographic emulsions. The effect of this bias is to suppress the number of large dip angles.

We have computed the ratio $N(|\beta| < 30^\circ)/N(|\beta| > 30^\circ) = 1.13 \pm 0.03$ from the experiments in connection with the apparent π-μ asymmetry.[36] If we compute the same ratio for all charged pions from the annihilation stars we obtain 1.22 ± 0.13. However if we consider only the pions missed by one or more of the observers, we obtain for the above ratio 0.75 ± 0.25. Here each pion was weighted by the number of observers who had missed it. Therefore our conclusion is that the deviation from unity we observe in the above ratio for all charged pions is due mainly to the same effect which led to the apparent π-μ asymmetry. In addition this effect is probably enhanced somewhat by the preferential missing of steep pions.

From the above analysis we are unable to evaluate the detection efficiency and we have to rely on estimates based on experience with decay products of μ, π and K mesons. We estimate the efficiency as $\epsilon = 0.90 \pm 0.05$. This estimate is in good agreement with the calculated value, if we assume charge independence, (see Section IV A).

As mentioned above, the efficiency of pion detection depends on grain density, and only pions with near minimum ionization escape detection. This has an influence on the pion spectrum and consequently on the average pion energy. We have corrected the pion spectrum by assuming no pion losses for $T_\pi < 100$ Mev ($g/g_o \gtrsim 1.24$) and ascribing all pion losses to pions with $T_\pi > 100$ Mev. This correction increases the measured average pion energy by a term w_2. We obtain $w_2 = 7 \pm 2$ Mev assuming $\epsilon = 0.90 \pm 0.05$ for all pions.

APPENDIX IV. IDENTIFICATION OF THE π MESONS

The identification of the light mesons emitted from antiproton stars is most easily accomplished for those mesons which come to rest in the stack. Measurements of multiple scattering and ionization on fast mesons are certainly sufficient to distinguish between light mesons and K mesons, but are not good enough to establish the light mesons as π or μ mesons.

In what follows, we give an analysis of the 76 light mesons followed to rest (53 negative, 22 positive and 1 of undetermined charge; see Section III A). We will now compare the terminal behavior of these particles with that of pions. In Fig. 22 the prong distribution of the 53 negative mesons is given. This is compared with an experimental distribution based on 4000 σ stars.[37] As can be seen from Fig. 22 the agreement is very good, leaving very little room for possible μ^- mesons which would occur as ρ mesons most likely. The average μ^+-meson range, from the 22 positive particles ($\pi^+\mu^+e^+$ decay), is 600.7 microns with a distribution in good agreement with the known[38] μ-meson distribution due to range straggling. There is no case of a direct μ^+-e^+ decay, thus ruling out the presence of a μ^+ particle among the 76 mesons considered here. In one case the charge could not be established. The track gives rise to either a short μ^+ (415 microns), and this gives a very low-energy decay electron (which would mean a π^+); or it is a π^--scattering event, in which the π^- ends in a π_ρ with a low-energy electron emission.

We have analyzed ionization-range measurements on 52 of these mesons selected on the basis of dip angle $\leq 50^\circ$ and no inelastic scattering of the tracks. The measurements consisted of counting 500 grains per track at the antiproton star and 500 grains for calibration of minimum ionization. From these measurements we obtain an average mass value of 148±4 Mev. The mass determination for the ρ mesons taken as a group gives 138±8 Mev, again leaving little room for μ^- contribution.

APPENDIX V. THE OBSERVATION OF A $K^+_{\mu 2}$ MESON

Among the antiproton stars observed in this experiment we have found one star, number 3-25 (Stack 72), which emits a K meson that comes to rest in the stack and decays. The decay secondary leaves the stack after traversing 147 plates. Figure 23 gives a microphotograph of the event. Track 1 is emitted at a dip angle of 30°; the particle comes to rest in the stack after traversing 34 plates and has a range of 3.9 cm (T_K = 87 Mev). On coming to rest track 1 gives off a secondary track 1'. Within the framework of the known particles our problem here is to distinguish between a K meson and a hyperon. Consequently we have only carried out relatively crude mass measurements. A direct grain count on more than 2000 grains gave $g/g_o = 2.37 \pm 0.11$ whereas a measurement of the gap coefficient[39] gave $g^* = 2.38 \pm 0.23$. In both cases g_o corresponds to 700 Mev pions which are essentially at minimum ionization. The corresponding masses are 760 ± 70 me and 745 ± 220 me respectively where the errors quoted are the statistical errors and do not contain systematic errors.

The secondary from particle 1, track 1', is emitted at a dip angle of 45°. Track 1' leaves the stack after traversing a distance of 11.6 cm through 147 plates. From ionization measurements on track 1' shown in Fig. 24, we can rule out a π meson from a $K_{\pi 2}$ meson. The multiple-scattering measurements on track 1' by the surface-angle method,[1] are shown in Fig. 25. Here we have also shown the expected variation of $p\beta$ versus distance from the decay point for a μ from a $K_{\mu 2}$, a π from a $K_{\pi 2}$ and an electron (emitted with maximum possible energy) from a K_{e3}, where the most probable energy loss (radiation and ionization) is plotted. It can be seen from Figs. 24 and 25 that the $K_{\mu 2}$ decay is the only one compatible with the measurements. It should be noted that a mass determination of track 1 based on the measurements of the secondary track 1' places that mass at the conventional value ($\sim 966\ m_e$) and so indicates that the low values obtained in the direct-mass measurements are most probably due to systematic errors.

The only additional prong (No. 2) emitted by the antiproton star comes to rest after 4.3 mm and is probably a proton of 33 Mev. There are also several Auger electrons emitted from this antiproton star.

APPENDIX VI. COMPILATION OF DATA ON PION INTERACTIONS IN PHOTOGRAPHIC EMULSIONS

One of the difficulties we encountered in the analysis of antiproton stars is the lack of information on pion interactions. By using data of pion interactions in photographic emulsions we get the proper mixture of light and heavy elements (at least to a good approximation) to compare directly with the case considered by us. For the analysis in Section IV we needed a number of quantities related to pion interactions. These are compiled and given in Table XI. In some cases the numbers needed were given directly by the authors; in other cases we deduced them from the available information. Finally we averaged the available quantities, with suitable interpolations and extrapolations, over the antiproton-annihilation spectrum assuming a primary π^+/π^- ratio of 0.76. The resulting average values for n_H, T_o, and (1-a) are given in the last row of Table XI.

Table XI

Compilation of Data on Pion Interactions in Photographic Emulsions

Column 3 gives the average number of heavy prongs n_H emitted in pion stars; this includes both absorption and inelastic scattering. Column 4 gives the average kinetic energy T_o of the inelastically scattered pions (this energy does not coincide with the peak energy, which is somewhat lower in general). Column 5 gives the percentage (1-a) of non-elastically interacting pions that give rise to inelastic scattering.

T_π Mev	Sign	n_H	T_o Mev	1-a %	Ref.
0	-	1.14			b
60-110	-		33	19	c
100	+	2.0	55	24.8±5	d
120	+	2.86	52.5	17.6±3	e
120	-	1.91	37	29.2±4	e
135	-		45	28 ±5	f
160	+		88±5		g
162	-		66±3	27.3±1.5	h
170	+	3.15		18.5±3.3	i
210	-	1.91	90	31 ±6	j
500[a]	-	4.23	110	38 ±6	k
Averaged		2.5±0.2	75±15	25±3	

a) Here ~ 1% of pion production is included
b) Marshak, Ref. 37.
c) Bernardini, Booth, Lederman, Tinlot, Phys. Rev. 82, 105 (1951).
d) Md. Shafi and D. J. Prowse, International Conference on Mesons and Recently Discovered Particles, Padua-Venice, September 1957, X-2.
e) Ferrari, Ferretti, Gessaroli, Manaresi, Pedretti, Puppi, Quareni, Ranzi, Stanghellini, and Stantic, Nuovo Cimento Suppl. 4, 914 (1956).
f) G. Goldhaber and S. Goldhaber, Phys. Rev. 91, 467 (1953) and additional unpublished data.
g) Nikol'skii, International Conference on Mesons and Recently Discovered Particles, Padua-Venice, September 1957, Nikol'skii, X-60.

Table XI (cont'd)

h) Nikol'skii, Kudrin and Ali-Zade, Soviet Phys. JETP. 5, 93 (1957).
i) Homa, Goldhaber and Lederman, Phys. Rev. 93, 554 (1954) and additional unpublished data.
j) A. H. Morrish, Phys. Rev. 90, 674 (1953).
k) M. Blau and M. Caulton, Phys. Rev. 96, 150 (1954).

REFERENCES

1. Barkas, Birge, Chupp, Ekspong, Goldhaber, Goldhaber, Heckman, Perkins, Sandweiss, Segrè, Smith, Stork, Van Rossum, Amaldi, Baroni, Castagnoli, Franzinetti, and Manfredini, Phys. Rev. 105, 1037 (1957).
2. A preliminary version of these results has been presented by Chamberlain, Goldhaber, Jauneau, Kalogeropoulos, Segrè, and Silberberg International Conference on Mesons and Recently Discovered Particles, Padua-Venice, September 1957, VI - 10.
3. We have not included in this analysis the work of Amaldi, Castagnoli, Ferro-Luzzi, Franzinetti, and Manfredini, Nuovo cimento 5, 1797 (1957);
   A.G. Ekspong, S. Johansson, and B.E. Ronnè, Nuovo cimento 8, 84 (1958); and
   A.H. Armstrong and G.M. Frye, Bull. Am. Phys. Soc. Ser. II, 2, 379 (1957), who have recently published results on 14, 10, and 16 antiproton stars respectively.
4. Z. Koba and G. Takeda, Progr. Theoret. Phys. (Kyoto) 19, 269 (1958).
5. E. Eberle, Nuovo cimento 8, 610 (1958).
6. T. Gotô, Nuovo cimento 8, 625 (1958).
7. S.Z. Belen'kii, Nuclear Phys. 2, 259 (1956).
8. M. Kretzschmar, Z. Physik 150, 247 (1958).
9. P.P. Srivastava and G. Sudarshan, Phys. Rev. 110, 765 (1958).
10. N. Yajima and K. Kobayakawa, Progr. Theoret. Phys. (Kyoto) 19, 192 (1958).
11. J.M. Blatt and V.F. Weisskopf Theoretical Nuclear Physics (Wiley New York, 1952), p. 346.
12. G. Goldhaber, T. Kalogeropoulos and R. Silberberg, Phys. Rev. 110, 1474 (1958).
13. G. Goldhaber and J. Sandweiss, Phys. Rev. 110, 1476 (1958).
14. The statistical error of $\langle N_\pi \rangle$ is evaluated as follows: assume that in all our stars we have n_1 with one prong, n_2 with 2 prongs, etc. Then in_i is the total number of prongs coming from stars with i prongs. In a large collection of stars we assume that n_i would have a Gaussian distribution with standard deviation $\sqrt{n_i}$. This gives the standard deviation for the total number of prongs, $(\sum_i i^2 n_i)^{1/2}$, and for the standard

deviation of the average multiplicity, $(\Sigma_i i^2 n_i)^{1/2}/\Sigma_i n_i$. Although this formula is not to be taken as exact, it probably is a good approximation. A similar method was used for the determination of the error of $\langle E_\pi \rangle$.

15. J. Sandweiss, On the Spin of K Mesons from the Analysis of Antiproton Annihilations in Nuclear Emulsions (Thesis) UCRL-3577, Oct. 1957.

16. Metropolis, Bivins, Storm, Miller, Friedlander, and Turkevich, Phys. Rev. 110, 204 (1958). Also private communcation from N. Metropolis.

17. K.J. LeCouteur, Proc. Phys. Soc. (London) A63, 259 and 498 (1950), A65, 718 (1952); also
Dostrovsky, Bivins, and Friedlander (unpublished calculations quoted in Ref. 16).

18. As in ACE we take a n/p ratio of 4 and assign each neutron the average kinetic energy T_n = 3 Mev, or the total energy E_n = 3+8=11 Mev. The resulting energy in evaporation prongs U_{ev} needs to be corrected for α particles present. This leads to a 15 to 18 % reduction in U_{ev}.

19. At T_π = 500 Mev, 1% charged-π-meson production was observed by Blau and Caulton (Phys. Rev. 96, 150 (1954)), and 3% was computed by Metropolis et al.[14]

20. From crude estimates we note, that the antiproton penetration into the nucleus is not sensitive to r_0, but would be very sensitive to the value of a.

21. Frank, Gammel and Watson, Phys. Rev. 101, 891 (1956).

22. Here we assume that, as far as the pion interactions are concerned, the nucleus can be treated as a uniform sphere of density ρ_o while, for the antiproton interactions, we take the shape given by ρ. The radius of the uniform sphere is thus tied to the values chosen for r_0 and a. The fraction of interacting pions 1-f has been given explicitly for uniform isotropic pion production throughout the spherical nucleus [Brueckner, Serber and Watson, Phys. Rev. 84, 258 (1951)] and for production on the surface of the nucleus [Webb, Iloff, Featherston, Chupp, Goldhaber and Goldhaber, Nuovo cimento 8, 899 (1958)] . We have evaluated f as a function of R_a by approximation methods.

23. Cork, Lambertson, Piccioni, Wenzel, Phys. Rev. 197, 248, (1957).

24. Agnew, Elioff, Fowler, Gilly, Lander, Oswald, Powell, Segrè, Steiner, White, Wiegand, and Ypsilantis, Phys. Rev. 110, 944, (1958).

25. E. Fermi, Progr. Theoret. Phys. (Kyoto) 5, 570 (1950); Belen'kii, Maksimenko, Nikisov, Rozenthal, Uspekhi Fiz. Nauk. 62, 1 (1957); G. Sudarshan, Phys. Rev. 103, 777 (1956).

26. F.J. Dyson, Phys. Rev. 99, 1037 (1957).

27. G.E.A. Fialho, Phys. Rev. 105, 328 (1957).

28. Horwitz, Miller, Murray, and Tripp, UCRL, private communication. See also the report by O. Piccioni at the 1958 Geneva High Energy Physics Conference (unpublished).

29. G.M. Frye (Phys. Rev. Letters 1, 14 (1958)) has observed a case of an antiproton giving a Dalitz pair and no ther charged prongs. Except for the Dalitz pair this corresponds to a $\bar{p}_\rho$.

30. T.D. Lee, Proceedings of the Seventh Annual Rochester Conference on High-Energy Nuclear Physics, VII, 1957, p. 12.

31. Chamberlain, Chupp, Ekspong, Goldhaber, Goldhaber, Lofgren, Segrè Wiegand, Amaldi, Baroni, Castagnoli, Franzinetti, and Manfredini, Phys. Rev. 102, 921 (1956).

32. Agnew, Chamberlain, Keller, Mermod, Rogers, Steiner, and Wiegand, Phys. Rev. 108, 1545 (1957).

33. In addition, we have observed what appears to be a $\bar{p}_\rho$ event (inside the rectangle of Fig. 21). This consists of a particle of protonic mass coming to rest (i.e., $T_{\bar{p}} < 10$ Mev); at a distance of 8μ from the ending we find a ten-prong star (including two pions). If these events are related, the neutral connecting particle was emitted at an angle of 92° with respect to the direction of the antiproton.

34. In this work no case of a disappearance in flight has been observed. Such cases have, however, been observed in new stacks (88 and 89) for which the scanning is now in progress.

35. Button, Elioff, Segrè, Steiner, Weingart, Wiegand and Ypsilantis, Phys. Rev. 108, 1557 (1957).

36. International Conference on Mesons and Recently Discovered Particles, Padua-Venice, September 1957 Lattes and Freier, IV-17; Ammar, Friedman, Levi Setti, Silvestrini, Slater, Telegdi, IV-24; Bhomwik, Evans and Prowse IV-35; Manfredini IV-38; Ferretti, Gessaroli, Lendinara, Minguzzi-Ranzi, Quareni-Vignudelli, and Quareni, IV-46.

37. The prong distribution of σ stars has been compiled by R. E. Marshak, "Meson Physics" P. 182, McGraw-Hill (1952) from the work of Menon, Muirhead and Rochat, Phil. Mag. 41, 583 (1950), and F. L. Adelman Phys. Rev. 85, 249 (1952).

38. W. F. Fry, Phys. Rev. 83, 1268 (1951); W. H. Barkas, Am. J. Phys. 20, 5 (1952).

39. P. H. Fowler and H. D. Perkins, Phil. Mag. 46, 587 (1955).

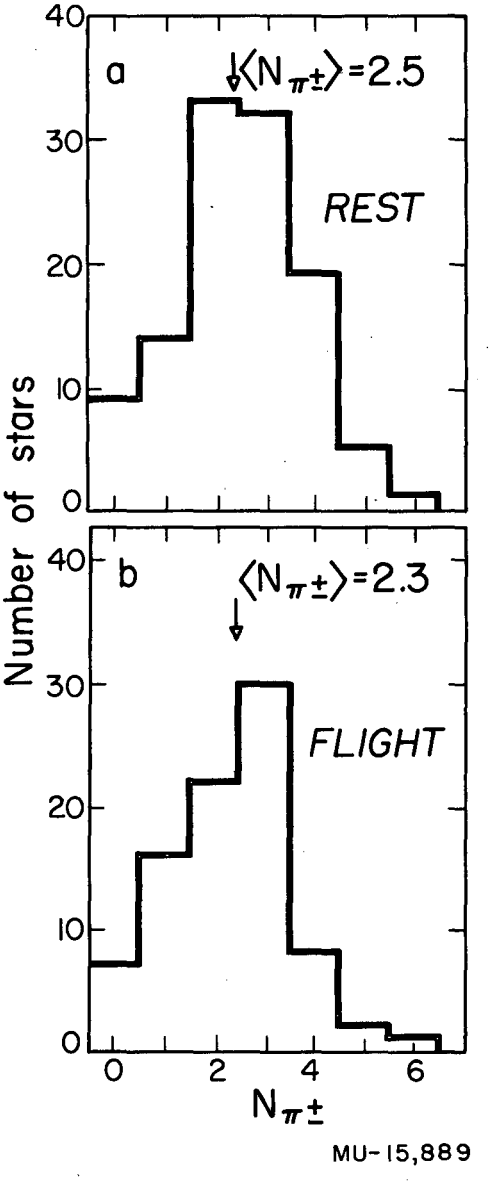

Fig. 1. The observed charged-pion multiplicity distribution from antiproton stars. In the upper diagram the data come from the stars at rest, in the lower diagram from the stars in flight. A similar separation is made in many of the other figures in this paper.

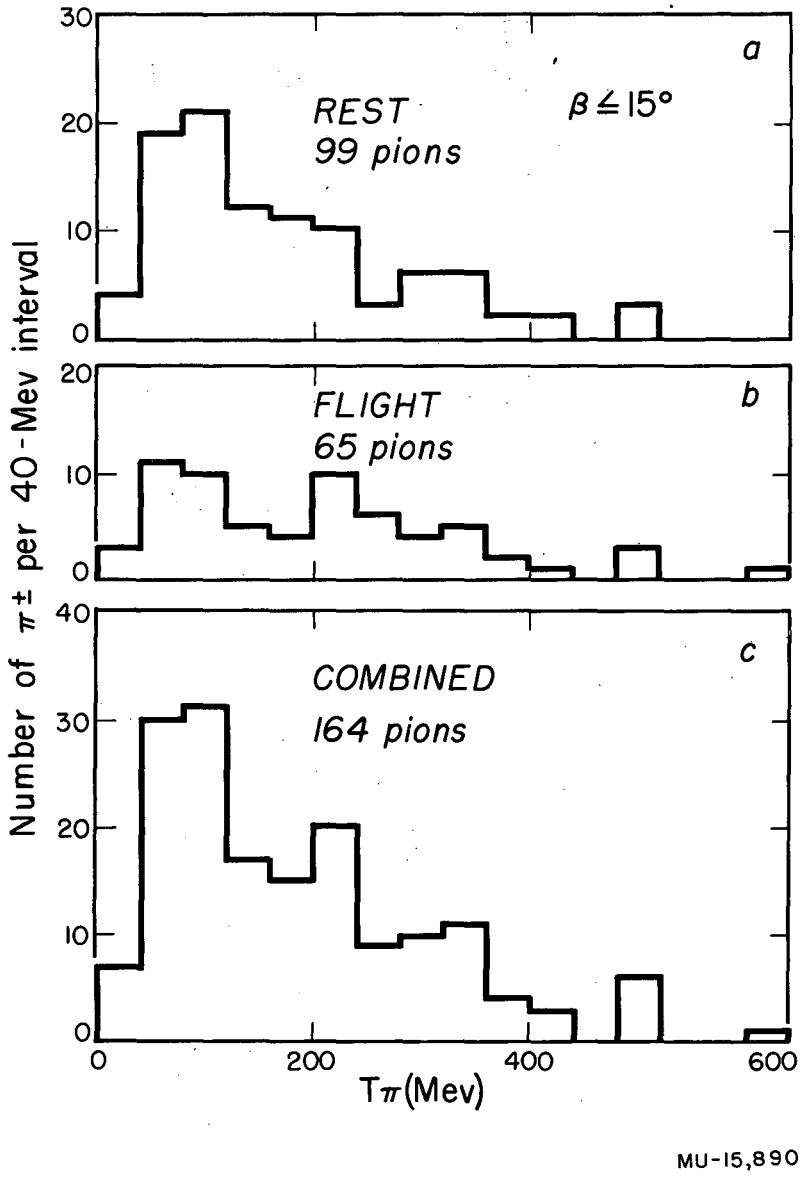

Fig. 2. The observed charged-pion spectrum from antiproton stars. Energy measurements included here come from pions with dip angle $\leq 15^{\circ}$. This represents $\sim 1/4$ of the total solid angle.

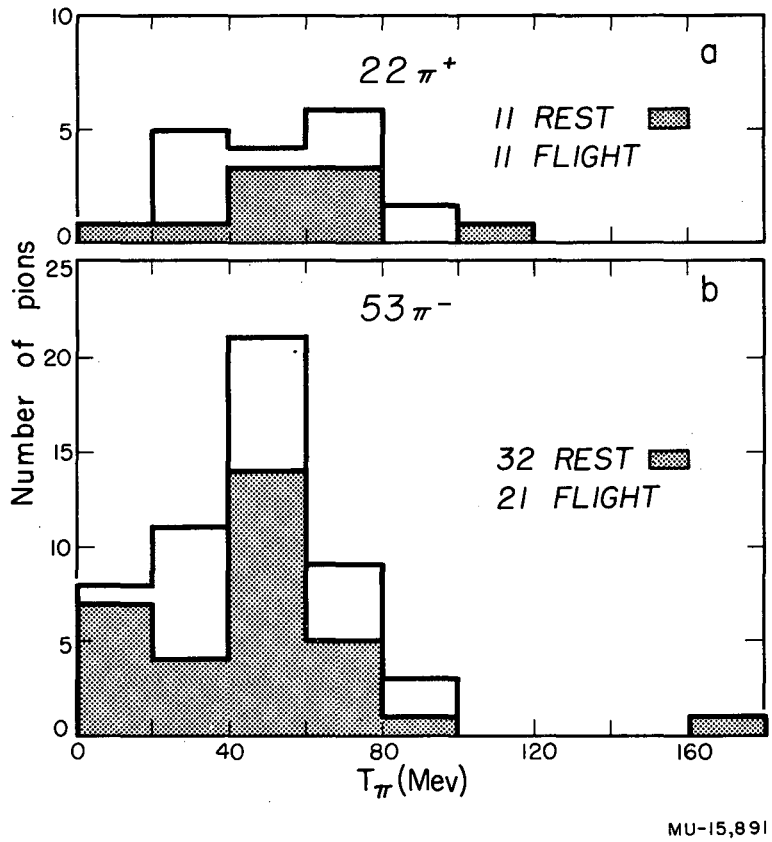

Fig. 3. The energy distribution of pions with identified sign from antiproton stars. The shaded histograms represent pions from antiproton stars at rest.

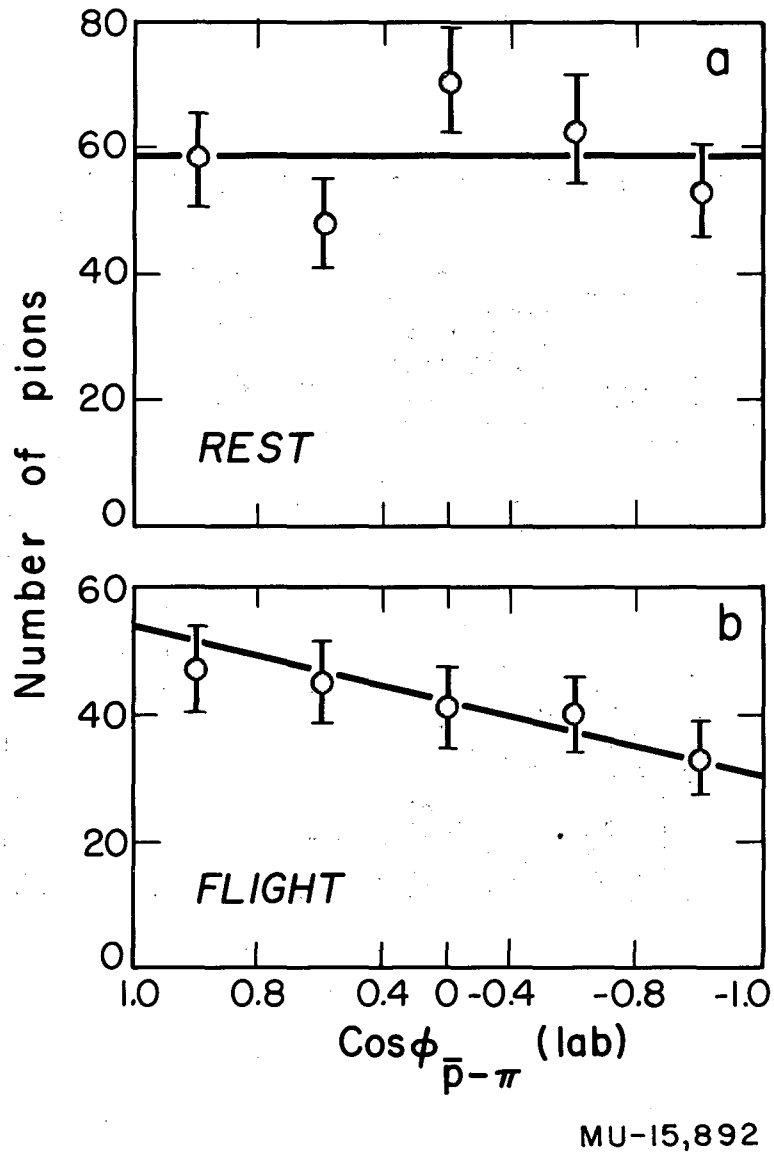

Fig. 4. The pion-emission angles relative to the antiproton direction in the laboratory system. The figure shows the number of pions plotted against the cosine of the emission angle. For the stars at rest, the line corresponding to isotropic emission is shown. For the stars in flight the line corresponding to isotropic emission in the c.m. system suitably averaged over antiproton and pion energies is shown.

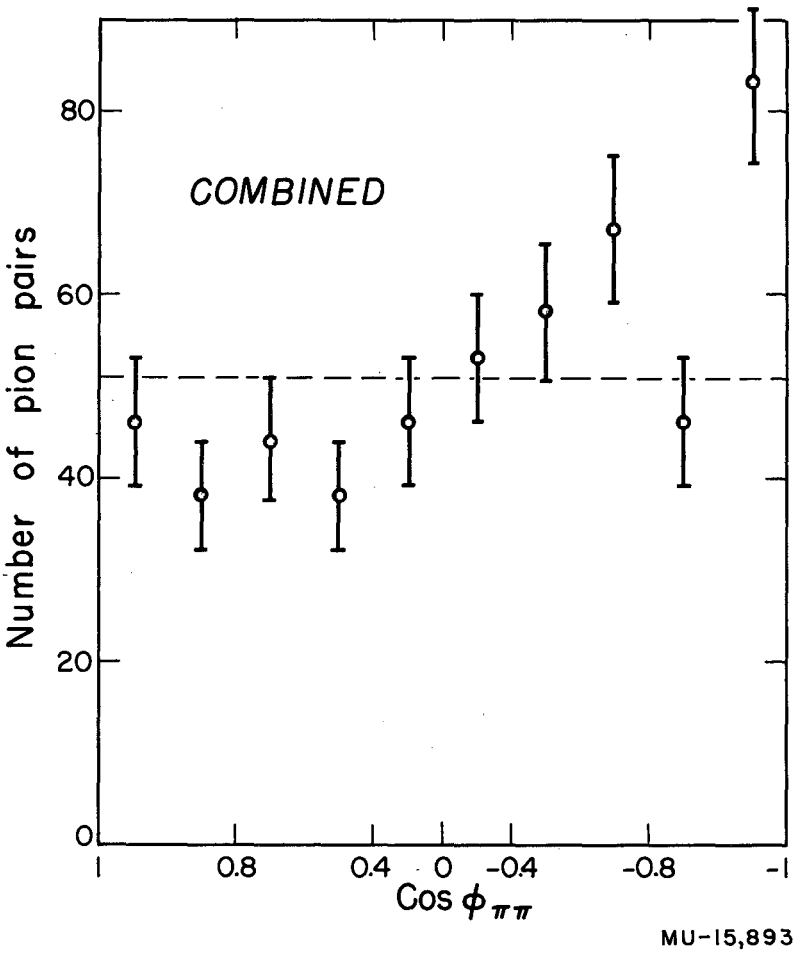

Fig. 5. The distribution of the angles between all pion-pion pairs from the antiproton-annihilation stars. The line corresponding to an isotropic distribution and thus no pion-pion correlation whatsoever, is also given.

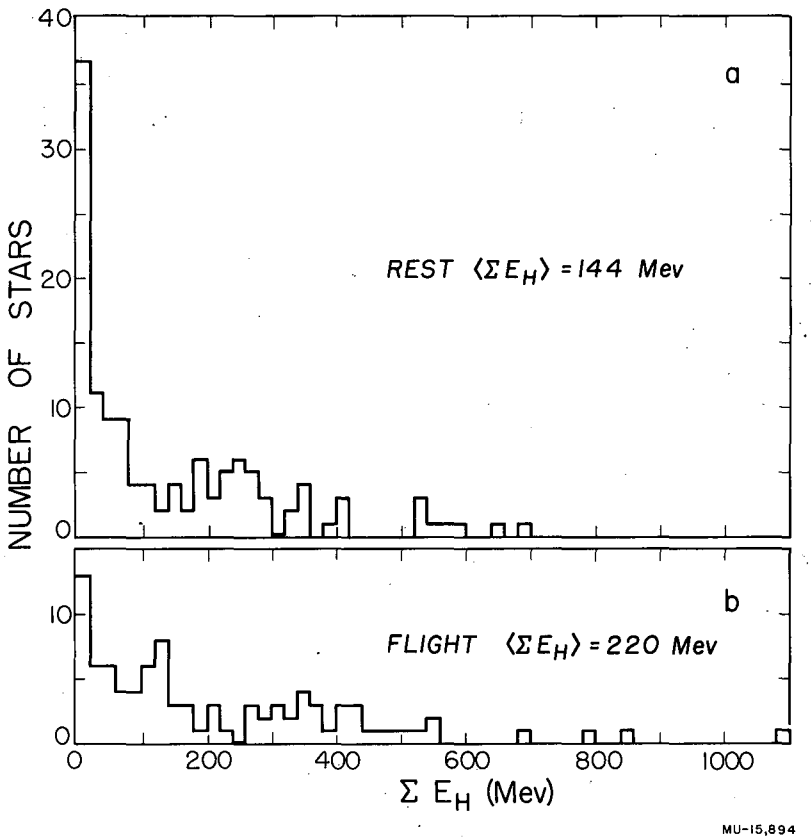

Fig. 6. The distribution of the energy emitted in heavy prongs (protons) per antiproton-annihilation star.

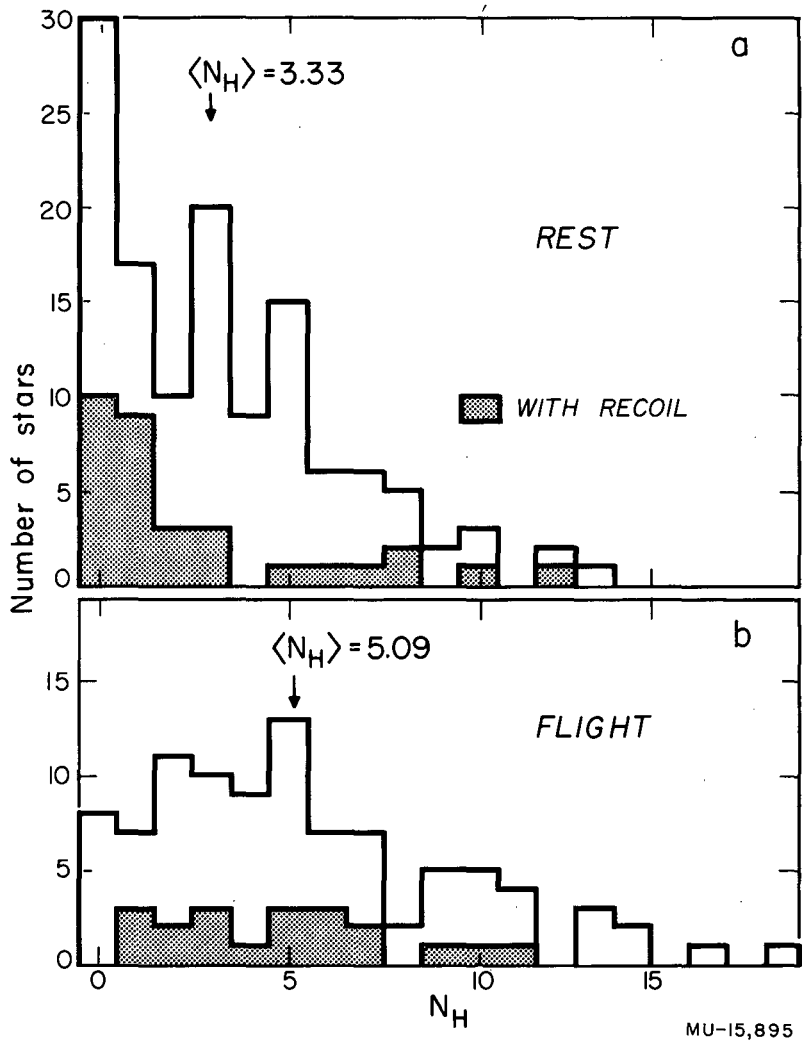

Fig. 7. The heavy-prong distribution from antiproton-annihilation stars.

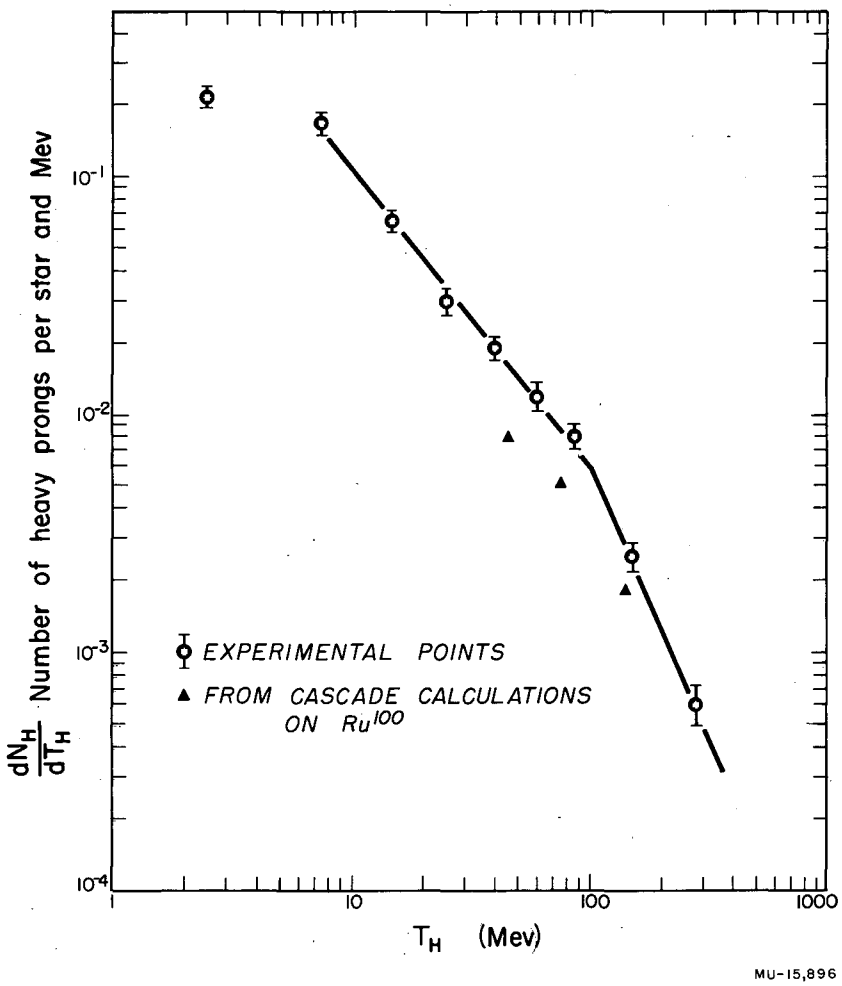

Fig. 8. The heavy-prong (proton) spectrum from antiproton-annihilation stars. The curve is an empirical fit to the data given in the text. The triangles are from cascade calculations on Ru^{100} by Metropolis et al.[16]

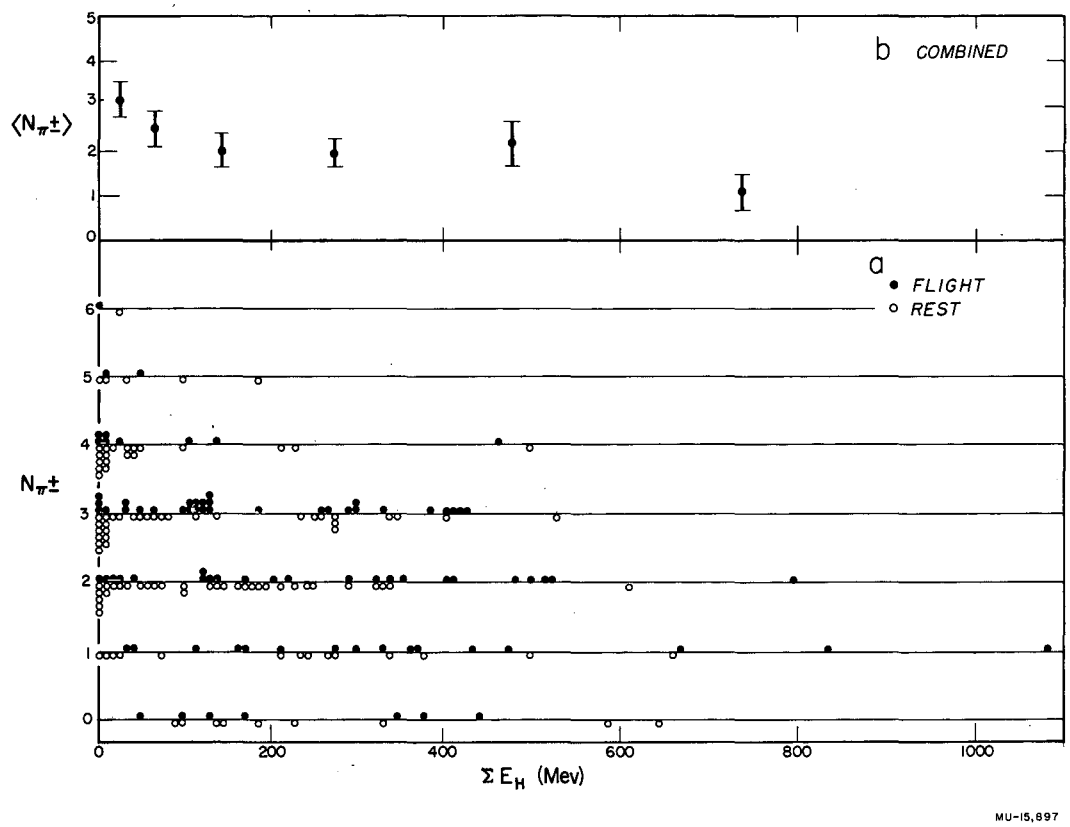

Fig. 9. (a) Correlation between energy given to heavy prongs $\{E_H$ and the observed charged-pion multiplicity $N\pi^{\pm}$ for antiproton-annihilation stars.

(b) The variation of the average charged-pion multiplicity $\langle N_{\pi^{\pm}} \rangle$ as a function of $\{E_H$.

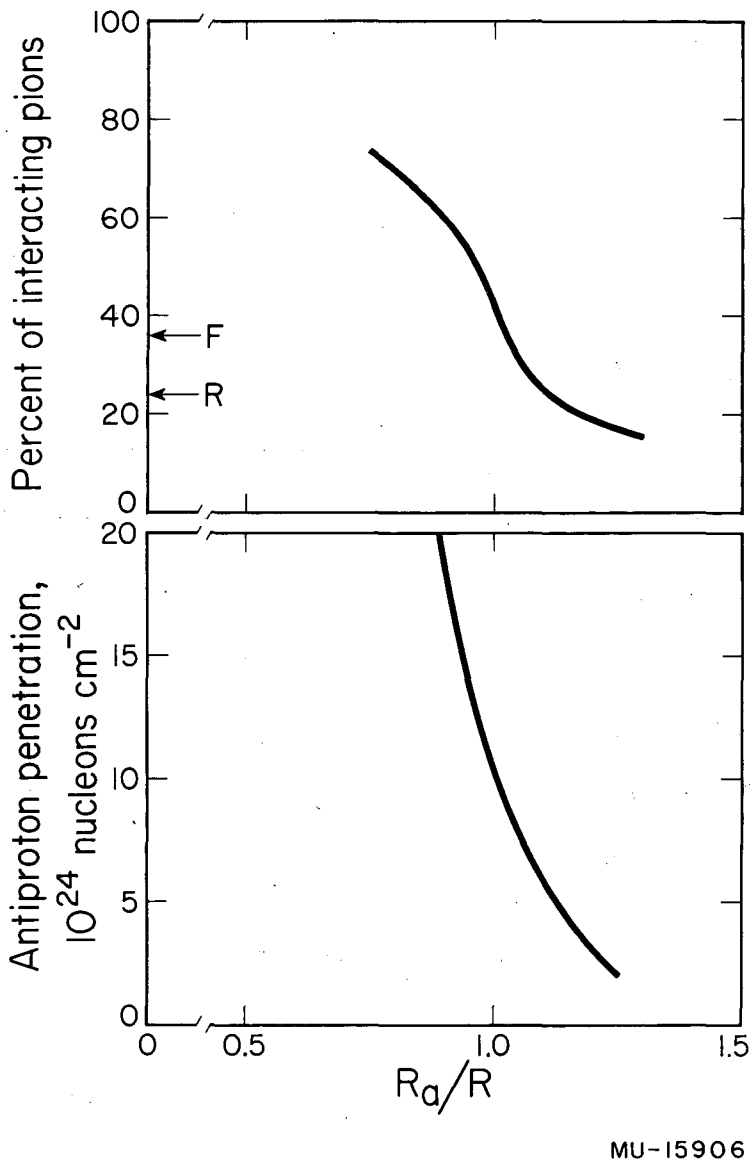

Fig. 10. (a) The percentage of interacting pions as a function of the average annihilation radius. The arrows marked R and F represent the percentage of interacting pions computed for stars at rest and in flight respectively.

(b) The average antiproton penetration depth into the nucleus as a function of the annihilation radius. Both curves are expressed in units of R, the half-density radius.

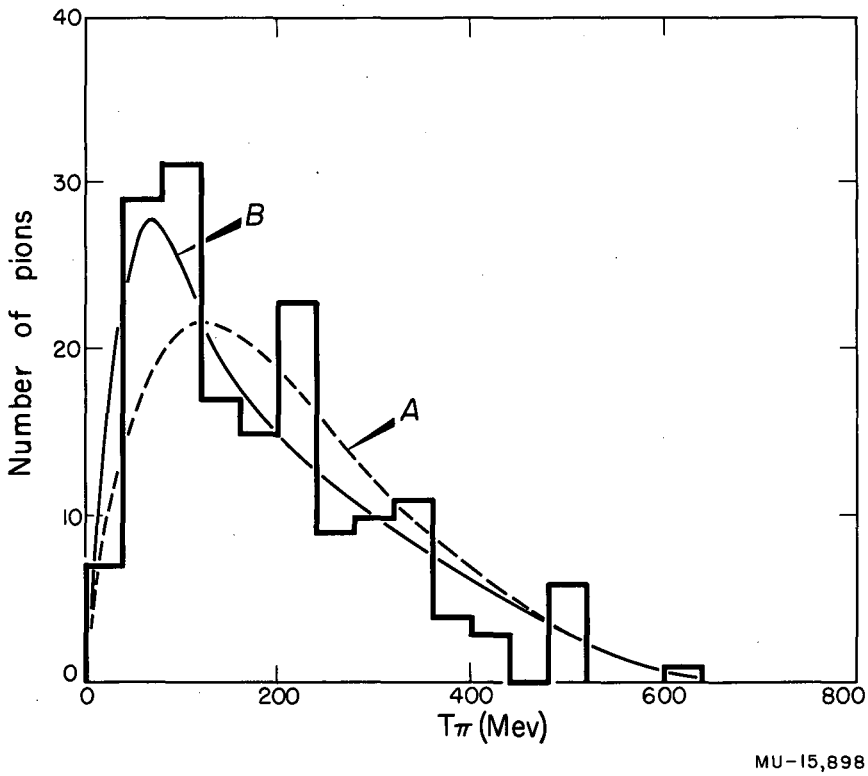

Fig. 11. The pion-energy spectrum. Curve A gives the pion-energy distribution as predicted by the normalized Fermi statistical model for $\langle N_\pi \rangle = 5.36$, and curve B gives this distribution corrected for the effects of pion absorption, inelastic scattering, and detection efficiency.

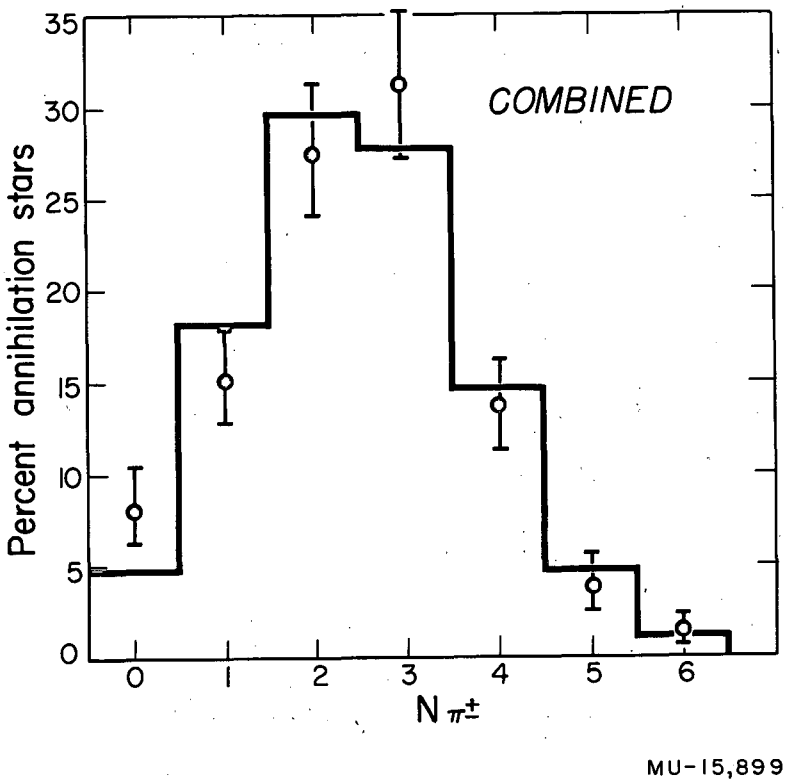

Fig. 12. The experimental charged-pion multiplicity distribution compared with the distribution of charged pions obtained from the normalized Fermi model for $\langle N_\pi \rangle = 5.36$, corrected for 32% loss through the effects of pion absorption and detection efficiency.

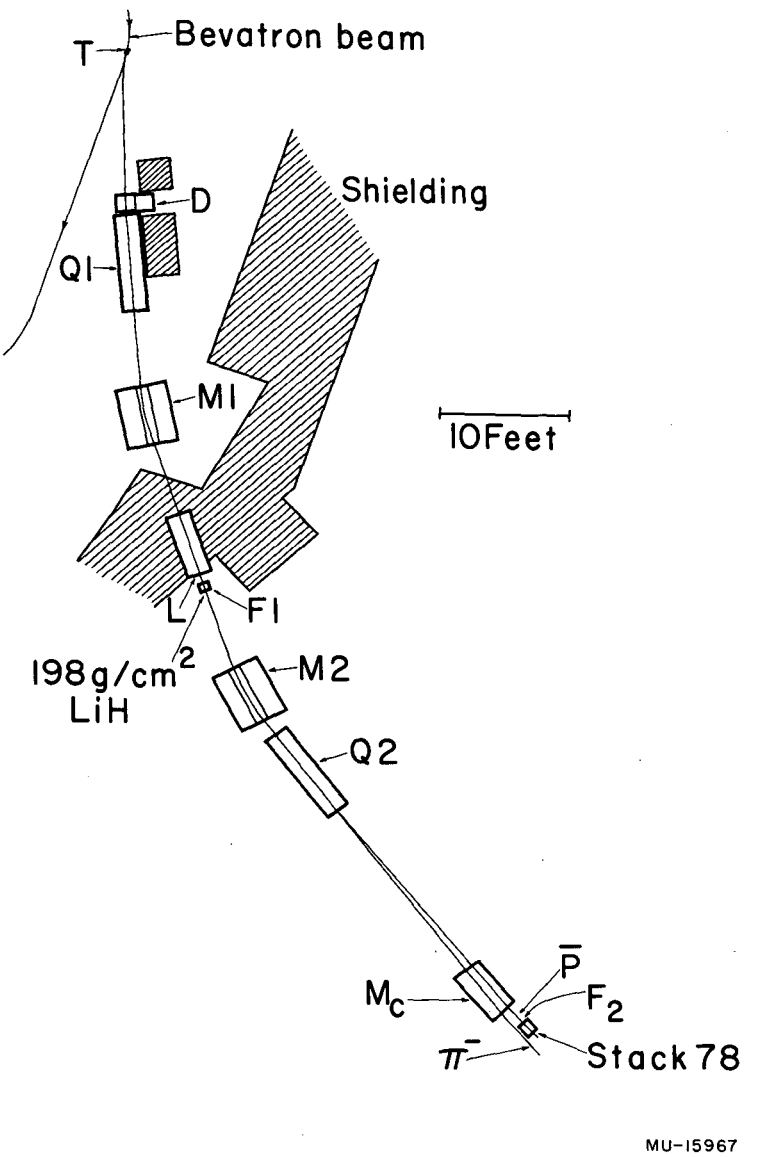

Fig. 13. The exposure geometry.

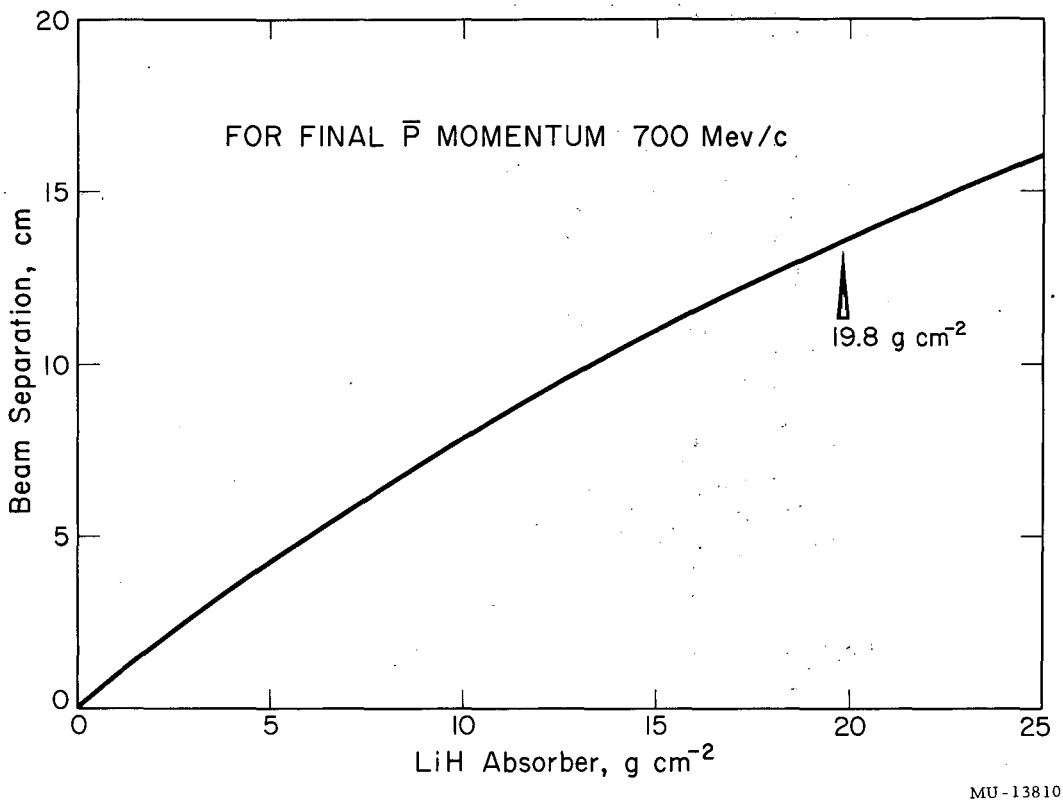

Fig. 14. The separation between the antiproton and pion beams as a function of lithium-hydride absorber thickness. This curve applies to the geometry shown in Fig. 13 and is for a final antiproton momentum of 700 Mev/c. The actual absorber used was 19.8 g/cm^2.

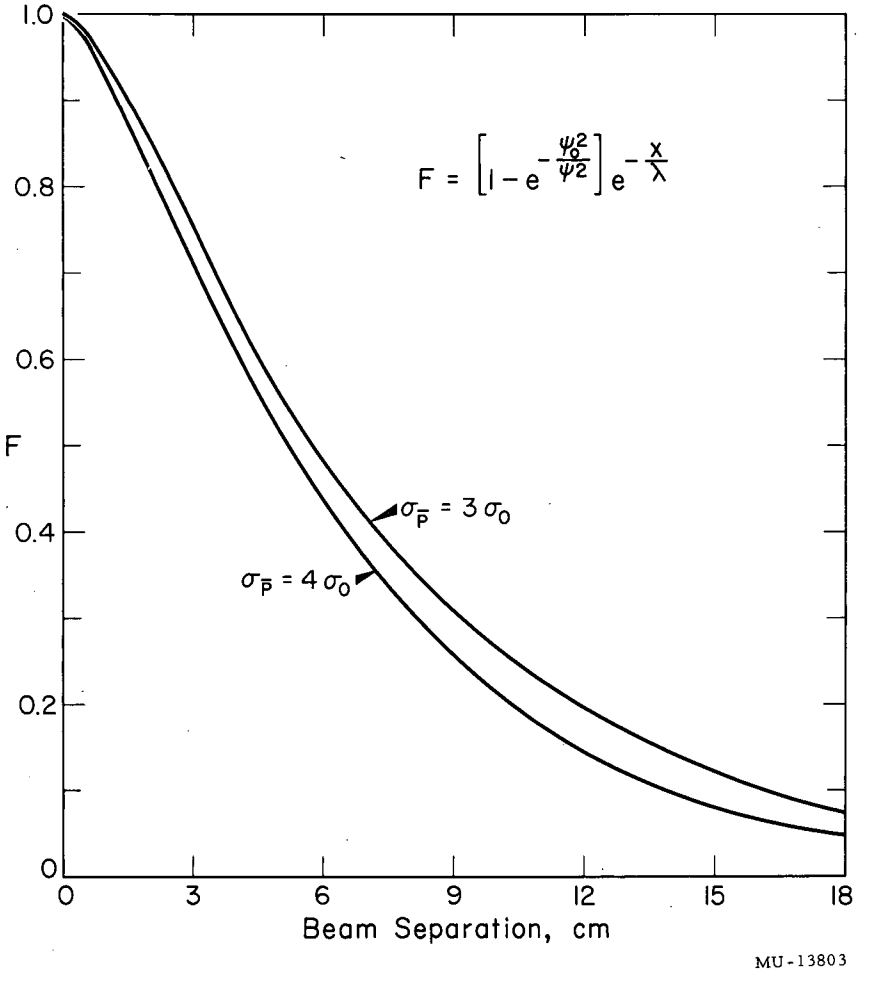

Fig. 15. The antiproton-reduction factor F as a function of antiproton-and pion-beam separation computed for the geometry shown in Fig. 13. The total antiproton cross section on lithium hydride down to a cutoff angle of 1^o has been estimated as lying between 3 and 4 times σ_0, where $\sigma_0 = \pi (1.2 \times 10^{-13} A^{1/3})^2$ cm^2.

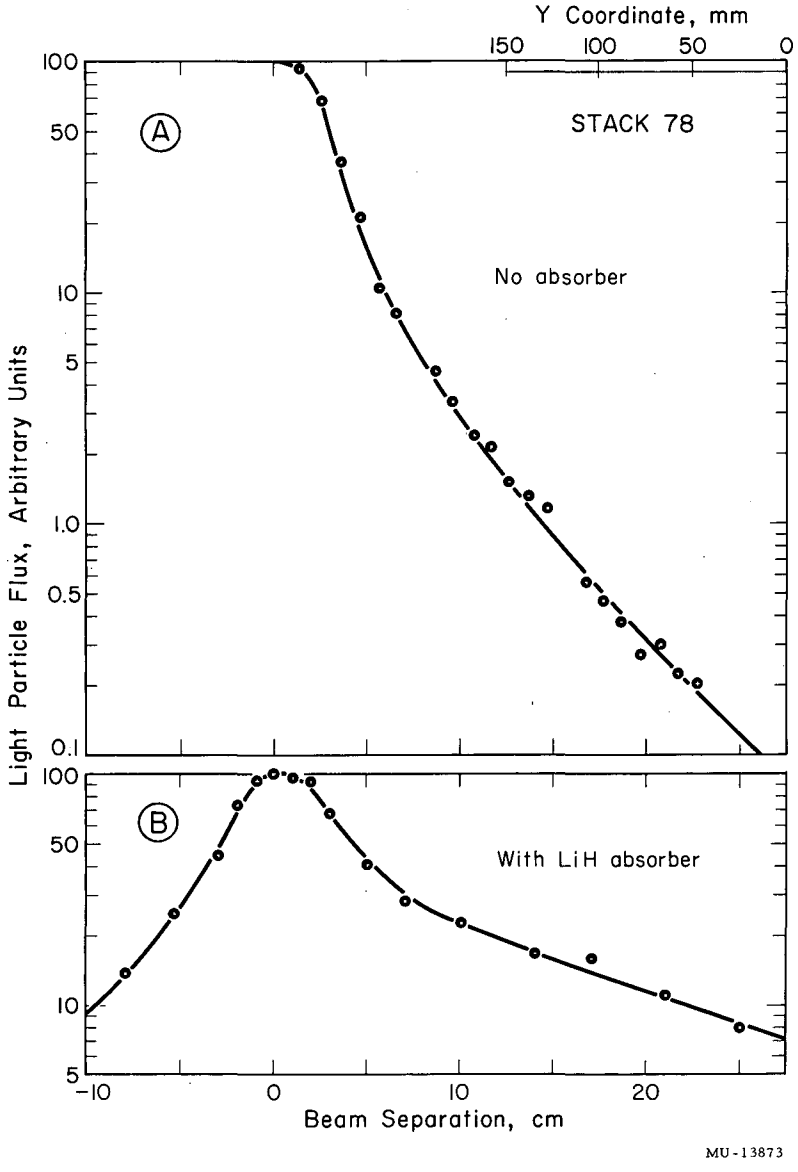

Fig. 16. The light-particle flux (π,μ, and e) in arbitrary units. The curve in Fig. 16 corresponds to the measurement without the lithium-hydride absorber in place. The curve in Fig. 16 corresponds to the measurement at the time of the exposure, with 19.8 g/cm^2 (24.9 cm) of lithium-hydride absorber in the beam. The flux measurements, carried out with test plates, have been normalized to 100 at the peak. The position of Stack 78 during the exposure and the grid coordinates on the emulsions are also shown at the top of Fig. 16.

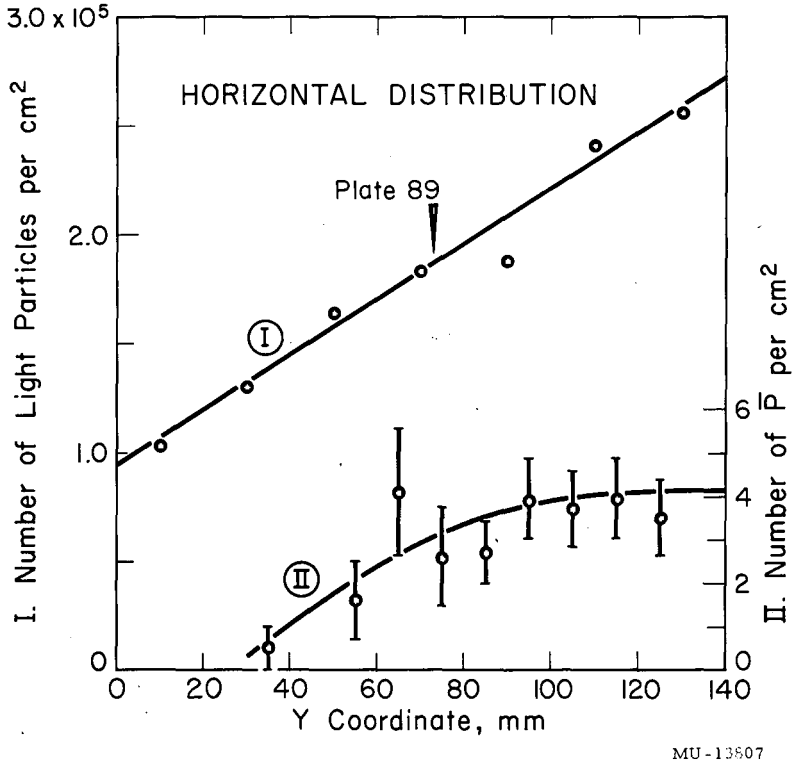

Fig. 17. The horizontal beam distribution in Stack 78. Curve I gives the light-particle flux as measured in Plate 89, a plate close to the peak of the vertical distribution. Curve II gives the antiproton flux as measured for Plates 50 to 130. A y coordinate of 125mm corresponds to a beam separation of 15cm as shown in Fig. 16.

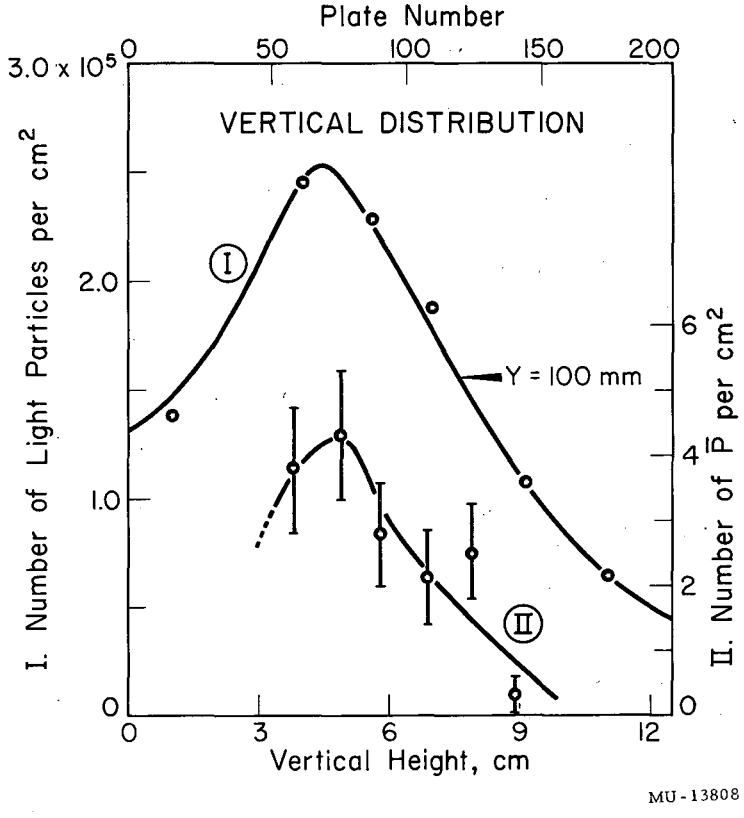

Fig. 18. The vertical-beam distribution in Stack 78. Curve I gives the light-particle flux as measured at y coordinate 100 in each plate of the stack. Curve II gives the antiproton flux as measured between Y coordinates 80 and 130.

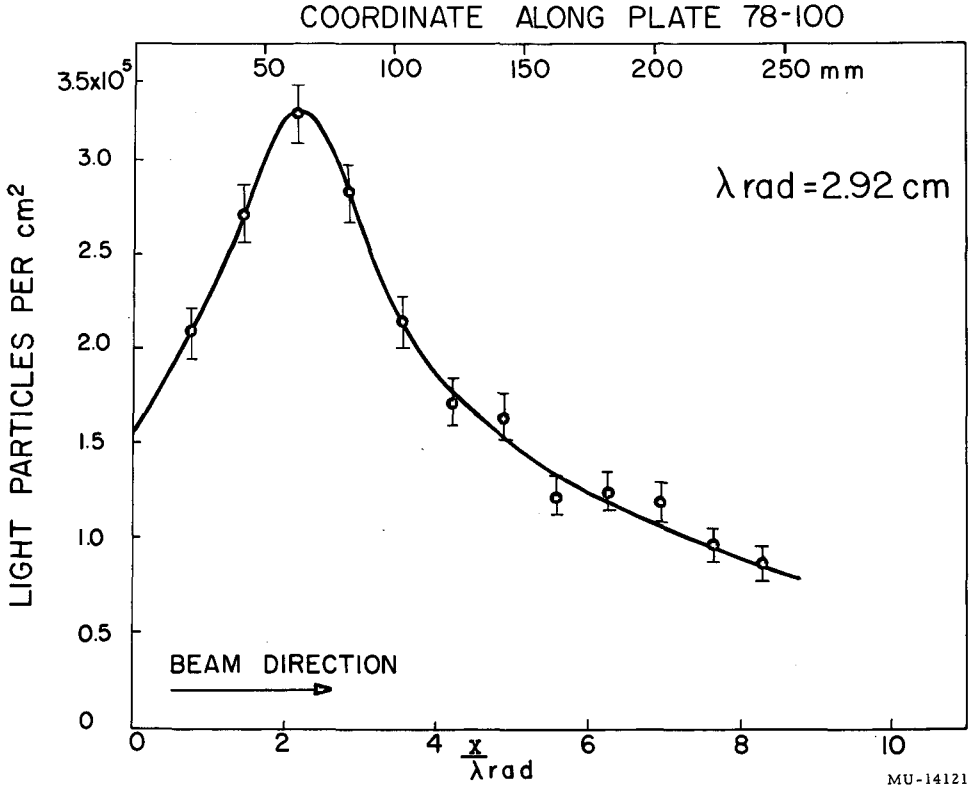

Fig. 19. The transition curve for the light-particle flux. The light-particle flux was measured along the beam direction (the X coordinate along Plate 78-100). The curve is plotted against distance along the plate as measured in radiation lengths in emulsion. The peak at about 2 units of radiation length clearly indicates the presence of a large fraction of electrons in the beam ($\sim$ 50 %).

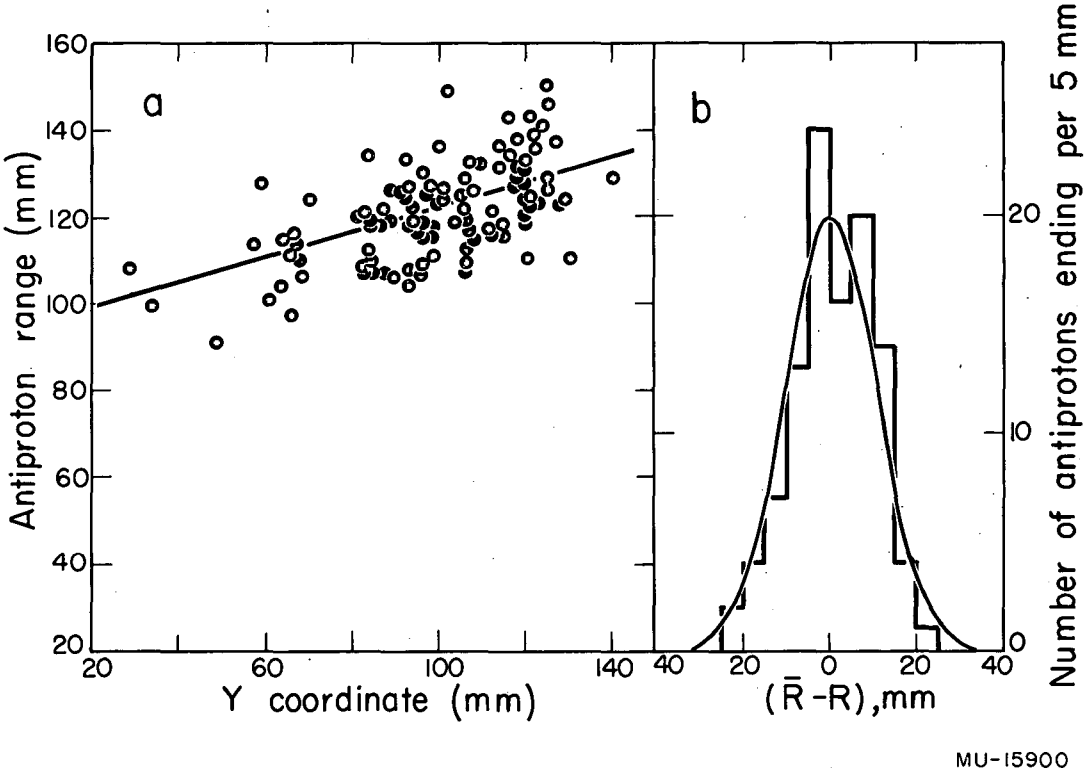

Fig. 20. (a) The range of stopping antiprotons is plotted as a function of the entrace y coordinate. The curve gives the mean antiproton range, $\bar{R}$ as a function of the y coordinate. The momentum dispersion is due to the clearing magnet M_C (see Fig. 13).

(b) The spread in range around $\bar{R}$ as given by the curve in A. The half width at half maximum is about 13 mm. $\Delta R/R$ is thus $\pm$ 0.11, which corresponds to a momentum spread of $\Delta P/P$ equal to $\pm$ 0.029.

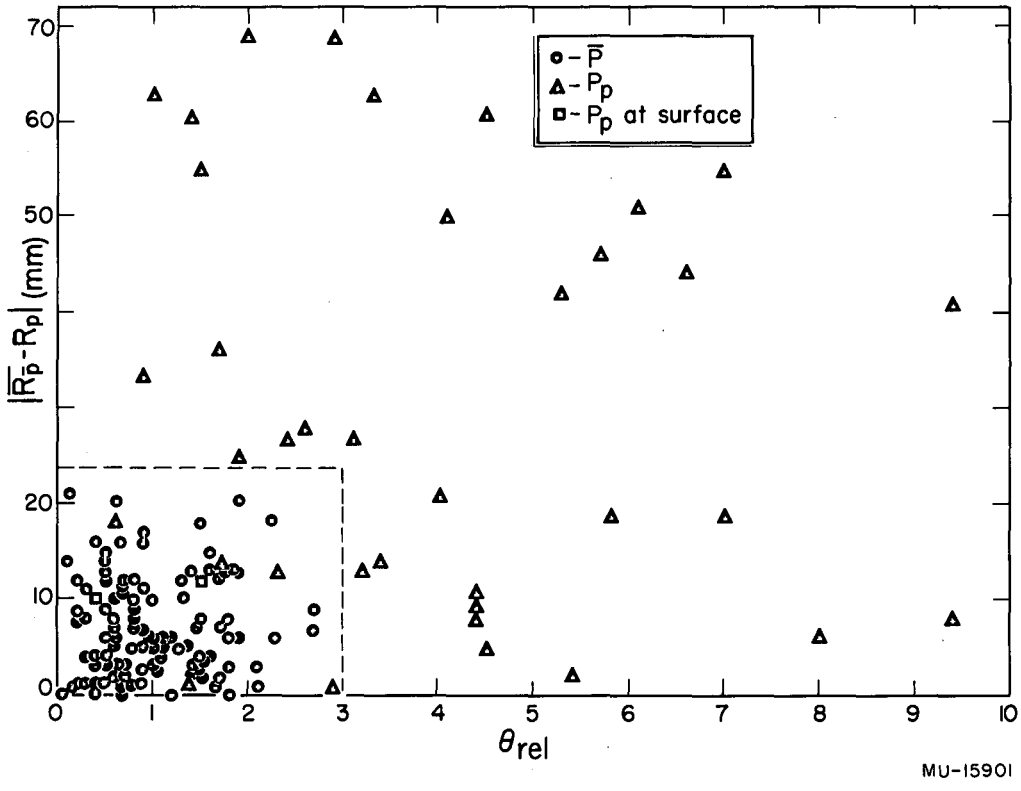

Fig. 21. A plot of the deviation in range from the mean range $\Delta R = |R - \bar{R}|$, for ending tracks of protonic mass versus the relative entrance angle θ_{rel} (space angle). The rectangle determined by $\theta_{rel} \leq 3^{\circ}$ and $\Delta R \leq 24$mm contains all the identified antiproton tracks.

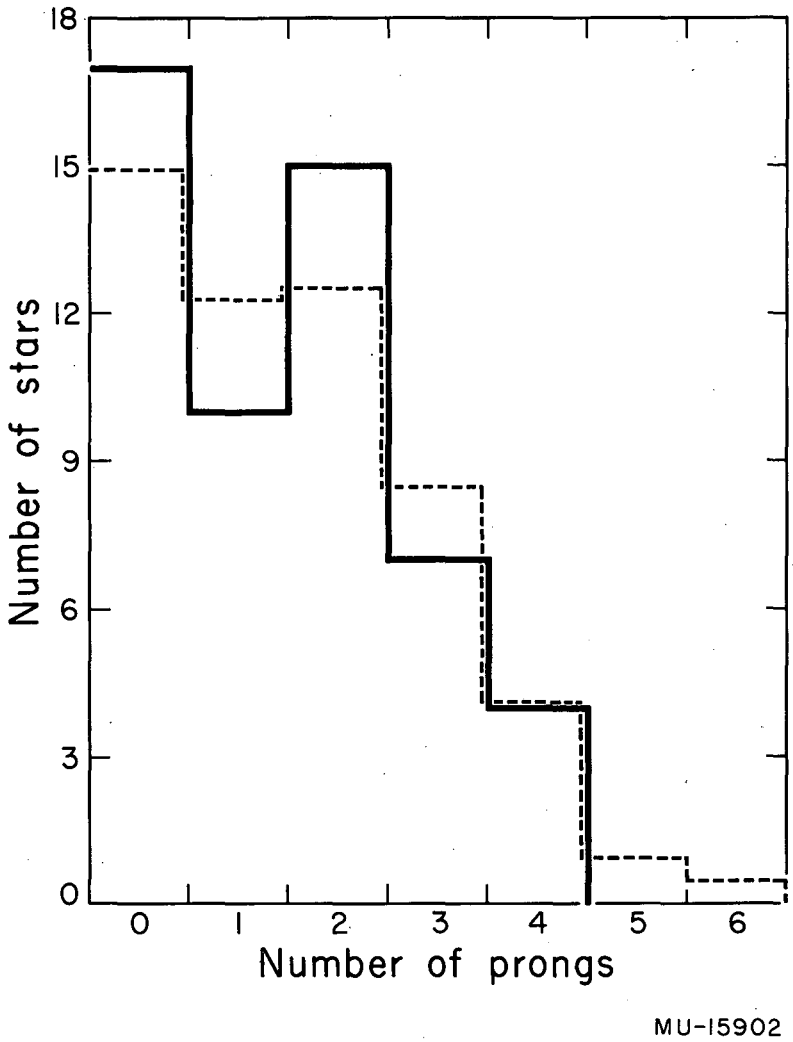

Fig. 22. The solid histogram gives the prong distribution of 53σ stars originating from antiproton-annihilation stars. The dashed histogram is the experimental prong distribution for 4000 π^- stars[37] normalized to 53.

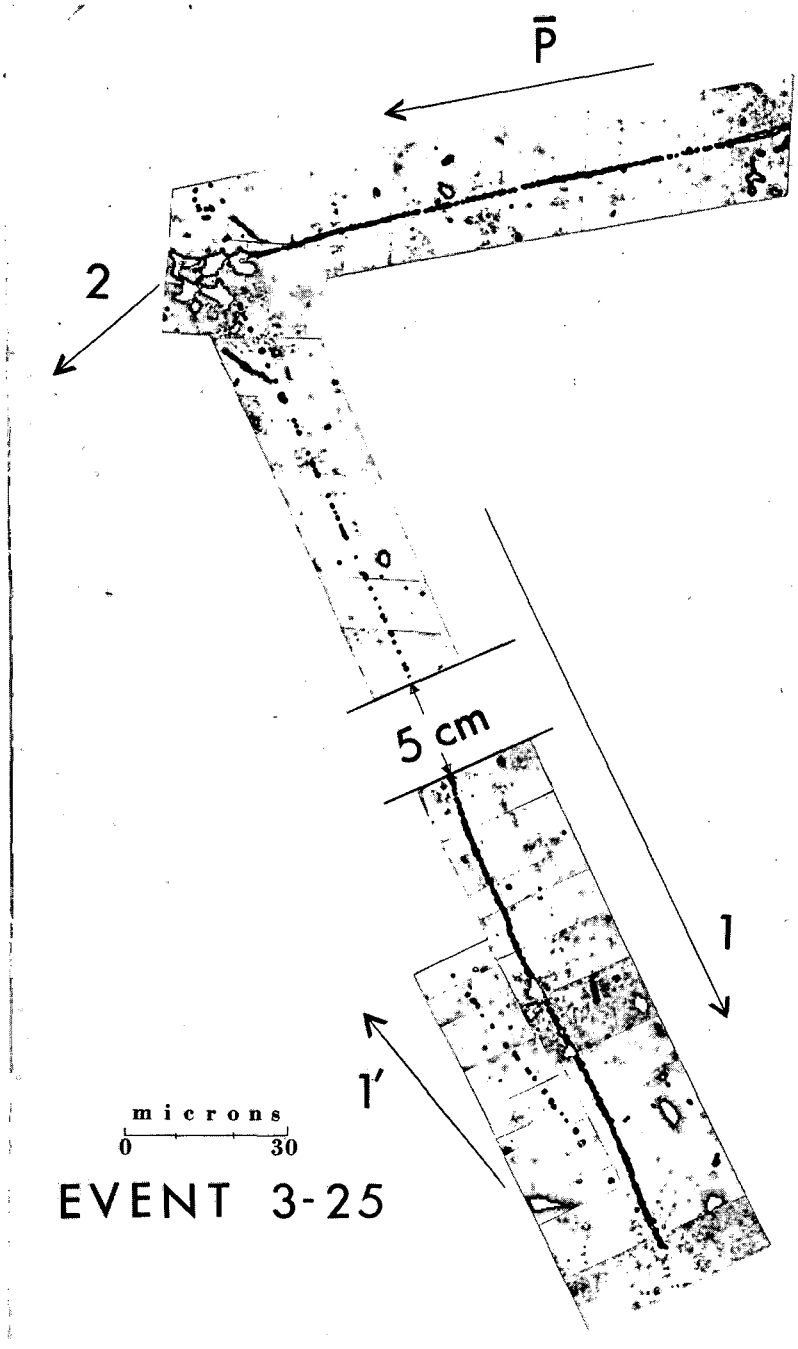

ZN-2018

Fig. 23. Photomicrograph of event 3-25, an antiproton-annihilation star emitting a $K^+\mu_2$ meson. Observer, Mrs. L. Shaw; photomicrograph by Mr. K. Natani. Track 2, which is very steep, was sketched in.

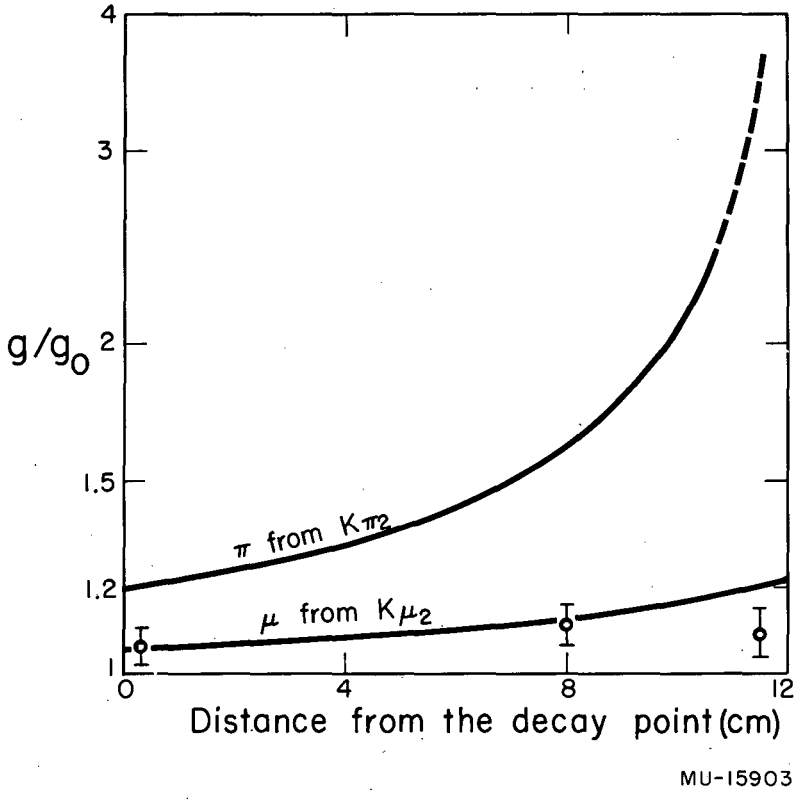

Fig. 24. Grain-count measurements on the secondary track 1'. The curves are the computed variation of grain count versus distance from the decay point for a π meson from a $K\pi_2$ and a μ meson from a $K\mu_2$.

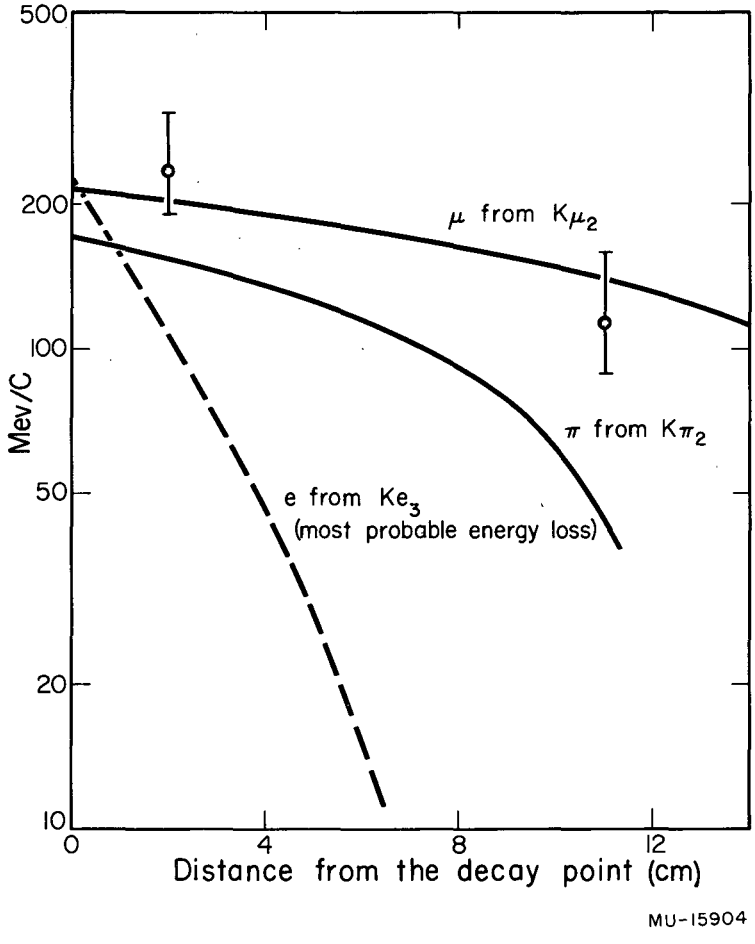

Fig. 25. Measurements of pβ on the secondary track 1'.